

Multidiffusion mechanisms for noble gases (He, Ne, Ar) in silicate glasses and melts in the transition temperature domain: Implications for glass polymerization

Julien Amalberti, Pete Burnard, Didier Laporte, Laurent Tissandier, Daniel R. Neuville

▶ **To cite this version:**

Julien Amalberti, Pete Burnard, Didier Laporte, Laurent Tissandier, Daniel R. Neuville. Multidiffusion mechanisms for noble gases (He, Ne, Ar) in silicate glasses and melts in the transition temperature domain: Implications for glass polymerization. Geochimica et Cosmochimica Acta, 2016, 172, pp.107-126. 10.1016/j.gca.2015.09.027 . hal-01636934

HAL Id: hal-01636934
https://uca.hal.science/hal-01636934

Submitted on 3 Sep 2021

HAL is a multi-disciplinary open access archive for the deposit and dissemination of scientific research documents, whether they are published or not. The documents may come from teaching and research institutions in France or abroad, or from public or private research centers.

L'archive ouverte pluridisciplinaire **HAL**, est destinée au dépôt et à la diffusion de documents scientifiques de niveau recherche, publiés ou non, émanant des établissements d'enseignement et de recherche français ou étrangers, des laboratoires publics ou privés.



Distributed under a Creative Commons Attribution 4.0 International License

Multidiffusion mechanisms for noble gases (He, Ne, Ar) in silicate glasses and melts in the transition temperature domain: Implications for glass polymerization

Julien Amalberti [a,1,*], Pete Burnard [a], Didier Laporte [b], Laurent Tissandier [a], Daniel R. Neuville [c]

[a] *Centre de Recherche Pétrographique et Géochimique, 15 Rue Notre-Dame des Pauvres, B.P.20, 54001 Vandoeuvre Cedex, France*
[b] *Laboratoire Magmas et Volcans, Université Blaise Pascal – CNRS – IRD, OPGC, 5 rue Kessler, 63038 Clermont-Ferrand, France*
[c] *Institut de Physique du Globe de paris, 1 rue Jussieu, 75005 Paris Cedex 05, France*

Noble gases are ideal probes to study the structure of silicate glasses and melts as the modifications of the silicate network induced by the incorporation of noble gases are negligible. In addition, there are systematic variations in noble gas atomic radii and several noble gas isotopes with which the influence of the network itself on diffusion may be investigated. Noble gases are therefore ideally suited to constrain the time scales of magma degassing and cooling. In order to document noble gas diffusion behavior in silicate glass, we measured the diffusivities of three noble gases (^{4}He, ^{20}Ne and ^{40}Ar) and the isotopic diffusivities of two Ar isotopes (^{36}Ar and ^{40}Ar) in two synthetic basaltic glasses (G1 and G2; ^{20}Ne and ^{36}Ar were only measured in sample G1). These new diffusion results are used to re-interpret time scales of the acquisition of fractionated atmospheric noble gas signatures in pumices.

The noble gas bearing glasses were synthesized by exposing the liquids to high noble gas partial pressures at high temperature and pressure (1750–1770 K and 1.2 GPa) in a piston-cylinder apparatus. Diffusivities were measured by step heating the glasses between 423 and 1198 K and measuring the fraction of gas released at each temperature step by noble gas mass spectrometry. In addition we measured the viscosity of G1 between 996 and 1072 K in order to determine the precise glass transition temperature and to estimate network relaxation time scales. The results indicate that, to a first order, that the smaller the size of the diffusing atom, the greater its diffusivity at a given temperature: D(He) > D(Ne) > D(Ar) at constant T. Significantly, the diffusivities of the noble gases in the glasses investigated do not display simple Arrhenian behavior: there are well-defined departures from Arrhenian behavior which occur at lower temperatures for He than for Ne or Ar. We propose that the non-Arrhenian behavior of noble gases can be explained by structural modifications of the silicate network itself as the glass transition temperature is approached: as the available free volume (available site for diffusive jumps) is modified, noble gas diffusion is no longer solely temperature-activated but also becomes sensitive to the kinetics of network rearrangements. The non-Arrhenian behavior of noble gas diffusion close to T_g is well described by a modified Vogel–Tammann–Fulcher (VTF) equation:

$$\frac{D}{a^2} = \frac{A_1}{a^2} * \exp\left(\frac{-B_1}{R(T - T_2)} - \frac{C}{RT}\right)$$

* Corresponding author.
E-mail address: jvamalbe@umich.edu (J. Amalberti).
[1] Current address: University of Michigan, Department of Earth and Environmental Sciences, Ann Arbor, MI, United States.

where D is the diffusion coefficient, a the diffusion domain size (taken to be the size of the sample), A_1 and C are respectively equivalent to the pre-exponential factor and to the activation energy (E_a in J mol^{-1}) of the classical Arrhenius equation, B_1 can be interpreted as a "pseudo-activation energy" that reflects the influence of the silicate network relaxation, T_2 is the temperature where the diffusion regime switches from Arrhenian to non-Arrhenian, and R is the gas constant (=8.314 J K^{-1} mol^{-1}).

Finally, our step heating diffusion experiments suggest that at T close to T_g, noble gas isotopes may suffer kinetic fractionation at a degree larger than that predicted by Graham's law. In the case of ^{40}Ar and ^{36}Ar, the traditional assumption based on Graham's law is that the ratio $D^{40}Ar/D^{36}Ar$ should be equal to 0.95 (the square root of the ratio of the mass of ^{36}Ar over the mass of ^{40}Ar). In our experiment with glass G1, $D^{40}Ar/D^{36}Ar$ rapidly decreased with decreasing temperature, from near unity (0.98 ± 0.14) at $T > 1040$ K to 0.76 when close to T_g ($T = 1003$ K). Replicate experiments are needed to confirm the strong kinetic fractionation of heavy noble gases close to the transition temperature.

1. INTRODUCTION

The solubility of volatile species (i.e. H_2O, CO_2, N_2, sulfur, the noble gases...) in magmas decreases with decreasing pressure. During ascent to the Earth's surface, magma will cross its volatile solubility limit at a certain pressure, the volatile saturation pressure, which depends on the initial concentrations of dissolved volatiles and below which bubbles will begin to form and grow. Bubble growth during decompression is fed by diffusion of gas from the melt to the volatile phase (Sparks, 1978). Therefore knowledge of the diffusion processes involved is required to understand and model magma degassing and volatile behavior under specific eruptive conditions. However, diffusion in silicate glass can be complex, frequently showing non-Arrhenian behavior around the glass transition temperature (Braedt and Frischat, 1988; Behrens, 1992; Caillot et al., 1994). Until now, non-Arrhenian diffusion has not been considered for volatiles (particularly noble gases) and its impact on magmatic degassing has not been evaluated. In order to better constrain diffusive processes in volcanic glasses, we undertook an experimental study investigating the diffusion of He, Ne and Ar (including Ar isotopes) in the CMAS (CaO-MgO-Al_2O_3-SiO_2) system over a broad temperature range (423–1198 K). Noble gases are chemically inert and do not form bonds that could affect the glass/liquid structure itself, so that they are ideal neutral tracers of the diffusion process. In addition, the noble gases have large and systematic changes in physical properties (diffusion, solubilities) and several isotopes that can be used to further constrain the process of diffusion in geological materials. The applications range from the time scales of magma degassing (e.g., Ruzié and Moreira, 2010) to the study of the origin and evolution of the Earth's volatiles (Moreira, 2013).

2. EXPERIMENTAL SET UP

2.1. Glass synthesis

CMAS glasses were prepared from a mixture of $CaCO_3$-MgO-Al_2O_3-SiO_2 powders. MgO, Al_2O_3, SiO_2 were dried at 1370 K and $CaCO_3$ at 820 K for 12 h, and mixed in the appropriate proportions to obtain a glass with 50 mol% of SiO_2, 9 mol% of Al_2O_3, 16 mol% of MgO and 25 mol% of CaO and one with 64.6 mol% of SiO_2, 15.9 mol% of Al_2O_3, 8 mol% MgO and 11.5 mol% of CaO (glasses G1 and G2, respectively). The mixture was then fused in a high temperature furnace at atmospheric pressure (at $T = 1820$ K) and quenched rapidly ($\sim$100 K s^{-1}) in order to obtain the CMAS glass. Fe-free compositions were chosen in order to simplify gas incorporation and understand diffusion mechanisms free from complications related to the redox state of iron, particularly as the Fe^{2+}/Fe^{3+} ratio is sensitive to temperature. However, our result can easily be applied to a Fe-bearing composition by assuming that Fe^{2+} corresponds to a network modifier or charge compensator such as Ca^{2+}, and Fe^{3+} behaves as a network former similar to Al^{3+} (Mysen et al., 1984; Kress and Carmichael, 1991; Magnien et al., 2006, 2008).

The CMAS glasses were doped with noble gases at high pressure-high temperature (HP-HT) in a piston-cylinder apparatus (in Laboratoire Magmas et Volcans, Clermont-Ferrand, France). We first loaded $\sim$20 mg of powdered glass into 3.0 mm outer diameter platinum capsules. Then we carefully added a noble gas mixture (2% Xe, 3% Kr, 5% Ar, 15% Ne and 75% He) using a loading device modified from Boettcher et al. (1989). A noble gas tank and a primary vacuum pump (1×10^{-3} mbar) were connected to the loading system. A manual valve controls the connection between the Pt capsule mounted in the loading system, the primary pump and the noble gas tank. The capsule was evacuated and then filled to 3 bars with the noble gas mixture then evacuated once more; this cycle was repeated three times so that the gas loaded in the capsule was as pure as possible. After the third cycle of charging the capsule with the noble gas mixture, the upper part of the Pt capsule was crimped in a vice to temporarily seal the gas in the capsule, and the gas-delivery system was disconnected. The capsule was then welded shut using a pulsed arc welder (PUK™) and finally removed from the vice.

The sealed capsules were equilibrated at temperatures between 1750 K and 1770 K and at a pressure of 1.2 GPa for 12 h in a non end-loaded, 3/4 inch piston-cylinder apparatus (see Laporte et al. (2004) for technical details). From the outside to the inside, the piston-cylinder assemblies consist of a NaCl cell wrapped in lead foil, a Pyrex cylinder, a graphite furnace, and inner pieces of compressible MgO powder. Temperature was controlled using calibrated

$W_{95}Re_5/W_{74}Re_{26}$ thermocouples. The experiments were terminated by shutting off the power to the apparatus; the quench rate was ~60 K/s.

2.2. Noble gas diffusion experiments

The noble gas diffusivities in the glasses were measured by *in vacuo* step heating (McDougall and Harrison, 1999) where noble gases are sequentially extracted at different temperatures. The noble gas analyses were performed at the Centre de Recherche Pétrographiques et Géochimiques, Nancy, France. The gas fraction, corresponding to a specific extraction time and temperature, allows the diffusivity at that temperature to be estimated (Carslaw and Jaeger, 1959; see also McDougall and Harrison, 1999). The extraction steps lasted between 10 and 40 min, at temperatures between 423 and 1198 K; the temperature resolution (difference in temperature between successive steps) was between 2 and 50 K (Table 1). The heating steps were performed in a halogen lamp furnace (Farley et al., 1999): temperature was monitored using a *K* thermocouple (Chromel/Alumel) located inside the molybdenum envelope containing the sample (uncertainties due to this procedure are estimated to be $<\pm 0.5$ K). The diffusion experiments were performed on glass fragments with radii *a* (±5%) of 0.35 mm and 1.075 mm for the G1 and G2 glasses, respectively (Table 1). These figures were obtained by measuring the maximum length of the glass fragments (D) on digitized photomicrographs and by converting them to radii ($a = D/2$). A full description of the diffusion measurement apparatus is given in Farley et al. (1999). At the end of the diffusion experiment, the samples were carefully transferred to a laser cell and melted using a CO_2 laser in order to measure the gas remaining in the glass after the step heating protocol.

Step heating is a convenient method for measuring noble gas diffusivities in a wide range of solid materials and over a large temperature range. The mathematical model used to compute the diffusion coefficient *D* from the fraction of gas *F* extracted during a temperature dwell of duration *t* (600, 1200 or 2400 s in this work; Table 1) is based on the assumptions that the sample is a spherical and that it has a uniform distribution of noble gases at the beginning of the experiment (Carslaw and Jaeger, 1959). The relationships between *F*, *t* and *D* have been derived in the case of a sphere of radius a for $F \geqslant 0.9$ by Fechtig and Kalbitzer (1966), and for $F \leqslant 0.1$ and $0.1 < F < 0.9$ by Reichenberg (1953):

$$F \leqslant 0.1 \qquad \mathrm{D/a^2} = \frac{F^2\pi}{36t} \tag{1a}$$

$$0.1 < F < 0.9 \qquad \frac{D}{a^2} = \frac{1}{\pi t}\left(2\pi - \frac{\pi}{3}F - 2\pi\sqrt{1-\frac{\pi}{3}F}\right) \tag{1b}$$

$$F \geqslant 0.9 \qquad \frac{D}{a^2} = -\frac{1}{\pi^2 t} ln\left(\frac{\pi^2}{6}(1-F)\right) \tag{1c}$$

Thus, knowing *F* and *t*, it is straightforward to compute the ratio D/a^2 for all temperature dwells. However, the samples used in this study are irregular fragments, as opposed to the perfect sphere assumed in the above equations. This non-spherical shape introduces a source of error in the calculations of D/a^2. Our irregular grains have angular corners with high-aspect ratios that will be rapidly drained of their noble gases during low-temperature extraction steps and are not expected to contribute significantly to the gas released at higher temperatures (Meesters and Dunai, 2002). Nevertheless, the first extraction steps (i.e. low F) of each particular sample are likely to be affected by the shape effect, and this will lead to overestimated diffusion coefficients at low temperatures as explained in Section 3.2.

The quantities of ^{4}He, ^{20}Ne, ^{36}Ar, and ^{40}Ar released were measured using a HELIX MC Plus™ Multi-collector Noble Gas Mass Spectrometer. Passive (T = room temperature) blanks were analyzed daily: ^{4}He and ^{20}Ne blanks were negligible ($<9 \times 10^{-16}$ mole), Ar blanks were $2.5 \times 10^{-14} \pm 1 \times 10^{-14}$ mole (1σ) over a 2 week period. An experiment was conducted in order to determine the high temperature (active) blanks: hot blanks (the same procedure as for sample analysis with the sole exception that no sample was loaded) were measured for durations of 20, 40 and 60 min, in order to better assess background contributions at high temperatures (Fig. 1). Significant ^{40}Ar blank contributions ($>9 \times 10^{-14}$ mole) are observed at high temperatures (~1000 K). For temperatures above 1000 K, the hot blanks were estimated by exponential extrapolation of the curves given in Fig. 1: these extrapolations yield blanks of $\sim 8 \times 10^{-13}$ mole ^{40}Ar at $T = 1200$ K. However, the glasses used for the diffusion experiments had sufficiently high noble gas contents so that the blank contribution remained small (<7%) even during the high temperature diffusion experiments.

In Table 1, the experimental results are expressed as ratios D/a^2. Knowing the radius a of the glass fragments in the step heating experiments, it is straightforward to extract the diffusion coefficient *D* from the ratio D/a^2. The error on sample size introduces an error into the diffusion coefficient estimate. Parameters *D* and a being the true diffusion coefficient and sample size, we call *a*' the measured sample size and *D*' the diffusion coefficient computed using *a*' instead of *a*. We introduce *a* parameter *e*, which is the relative error on sample size: $a' = a \pm e \times a = a \times (1 \pm e)$. Thus the expression for *D*' is: $D' = D \times (a'/a)^2 = D \times (1 \pm e)^2$. For a 5% error on sample size ($e = 0.05$), the relative error on the calculated diffusivities would be $(D' - D)/D = (1 \pm e)^2 - 1 \sim \pm 10\%$. We estimate that the error on sample size introduces a maximum uncertainty of ±10% on diffusion coefficients.

2.3. Viscosity experiments

The viscosity of the glass G1 was measured as a function of temperature to determine its glass transition temperature (T_g). A new batch of glass G1 free of noble gases was synthesized in a 1-atmosphere furnace and quenched at ~100 K s^{-1}. In order to made viscosity measurement, the glass sample was a cylinder of 5.5 mm diameter and of initial length of c. 9 mm. The measurements were made between 997 and 1072 K using a creep apparatus of the Institut de Physique du Globe

Table 1
Step heating data for ^{4}He, ^{20}Ne, ^{36}Ar and ^{40}Ar in glass G1 and G2 and the calculated diffusivities.

Temperature (K)	Time (s) Ar/He[+ e]	^{40}Ar[c]			^{4}He[c]		
		Gas[a]	D/a^2	F[b] (%)	Gas[a]	D/a^2	F[b] (%)
G2 glass							
473	600^{+}	–	–	–	1.37×10^{-09}	$2.28 \times 10^{-07*}$	4
533	600^{+}	–	–	–	2.12×10^{-09}	6.39×10^{-07}	6.5
548	600^{+}	–	–	–	6.67×10^{-09}	3.33×10^{-06}	14.5
573	600^{+}	–	–	–	4.57×10^{-09}	6.54×10^{-06}	20
623	600^{+}	–	–	–	8.34×10^{-09}	1.57×10^{-05}	30
648	600^{+}	–	–	–	1.16×10^{-08}	3.75×10^{-05}	44
673	600^{+}	–	–	–	1.14×10^{-08}	7.31×10^{-05}	57.6
698	600^{+}	–	–	–	1.22×10^{-08}	1.37×10^{-04}	72.4
723	2400600^{+}	$1.38 \times 10^{-12}(<1 \times 10^{-14})$	$1.08 \times 10^{-13*}$	0.01	8.56×10^{-09}	2.13×10^{-04}	82.7
748	2400600^{+}	$7.50 \times 10^{-13}(<1 \times 10^{-14})$	$2.58 \times 10^{-13*}$	0.01	6.69×10^{-09}	3.17×10^{-04}	90.7
773	2400600^{+}	$1.20 \times 10^{-12}(<1 \times 10^{-14})$	$6.30 \times 10^{-13*}$	0.01	3.97×10^{-09}	4.39×10^{-04}	95.5
798	600^{+}	–	–	–	1.85×10^{-09}	5.54×10^{-04}	97.7
823	2400600^{+}	2.96×10^{-12} ($<1 \times 10^{-14}$)	$7.1 \times 10^{-13*}$	0.02	8.76×10^{-10}	6.58×10^{-04}	98.8
873	2400600^{+}	5.38×10^{-12} ($<1 \times 10^{-14}$)	$7.74 \times 10^{-12*}$	0.05	3.44×10^{-10}	7.27×10^{-04}	99.2
898	2400600^{+}	3.88×10^{-12} ($<1 \times 10^{-14}$)	$1.38 \times 10^{-11*}$	0.06	1.42×10^{-10}	7.67×10^{-04}	99.4
923	2400600^{+}	1.66×10^{-11} ($<1 \times 10^{-14}$)	5.88×10^{-11}	0.13	7.88×10^{-11}	7.94×10^{-04}	99.5
948	2400600^{+}	1.69×10^{-11} (5.7×10^{-14})	1.37×10^{-10}	0.19	6.10×10^{-11}	8.18×10^{-04}	99.5
973	2400/600	3.65×10^{-11} (1.2×10^{-13})	4.16×10^{-10}	0.34	5.64×10^{-11}	8.44×10^{-04}	99.6
1023	2400600^{+}	2.27×10^{-10} (4.1×10^{-13})	5.56×10^{-09}	1.24	–	–	–
1073	2400600^{+}	2.39×10^{-10} (9.9×10^{-13})	3.46×10^{-08}	2.18	–	–	–
1123	2400600^{+}	8.16×10^{-10} (1.8×10^{-12})	2.19×10^{-07}	5.4	–	–	–
1173	1200600^{+}	3.17×10^{-09} (3.4×10^{-12})	2.59×10^{-06}	18	–	–	–
1198	1200600^{+}	1.51×10^{-08} (4.0×10^{-12})	8.54×10^{-05}	77.6	–	–	–
CO_2 laser extraction:		$5.7 \times 10^{-09}(<1.0 \times 10^{-17})$			3.42×10^{-10}		
Total:		2.53×10^{-08}			8.31×10^{-08}		
G1 glass							
		^{4}He[d]			^{20}Ne[d]		
		Gas[a]	D/a^2	F[b] (%)	Gas[a]	D/a^2	F[b] (%)
423	2400	2.32×10^{-11}	$1.83 \times 10^{-10*}$	0.33	7.55×10^{-14}	$1.36 \times 10^{-14*}$	0.00
473	2400	1.58×10^{-10}	4.05×10^{-10}	2.61	2.53×10^{-12}	$1.61 \times 10^{-11*}$	0.07
523	2400	2.05×10^{-10}	2.48×10^{-08}	5.56	3.14×10^{-12}	$7.85 \times 10^{-11*}$	0.15
573	2400	3.76×10^{-10}	1.16×10^{-07}	10.97	7.34×10^{-12}	$4.07 \times 10^{-10*}$	0.33
653	2400	7.96×10^{-10}	2.08×10^{-06}	22.43	1.82×10^{-11}	4.35×10^{-08}	3.46
703	2400	1.14×10^{-09}	7.02×10^{-06}	38.89	2.77×10^{-11}	6.32×10^{-08}	4.17
723	2400	6.72×10^{-10}	1.19×10^{-05}	48.56	3.61×10^{-11}	9.68×10^{-08}	5.09
773	2400	1.04×10^{-09}	2.36×10^{-05}	63.59	4.07×10^{-11}	1.41×10^{-07}	6.13
823	2400	9.34×10^{-10}	4.17×10^{-05}	77.05	8.58×10^{-11}	2.64×10^{-07}	8.32
863	2400	6.43×10^{-10}	6.31×10^{-05}	86.31	1.15×10^{-10}	4.91×10^{-07}	11.3
923	2400	7.01×10^{-10}	1.19×10^{-04}	96.39	3.49×10^{-10}	1.67×10^{-06}	20.2

963	2400	1.54×10^{-10}	1.59×10^{-04}	98.61	3.34×10^{-10}	3.57×10^{-06}	28.6
1003	2400	2.64×10^{-11}	1.73×10^{-04}	98.99	3.61×10^{-10}	6.65×10^{-06}	38.0
1023	2400	2.11×10^{-11}	1.88×10^{-04}	99.29	5.37×10^{-11}	7.22×10^{-06}	39.4
1039	2400	6.54×10^{-12}	1.94×10^{-04}	99.39	1.05×10^{-10}	8.41×10^{-06}	42.0
1041	2400	4.34×10^{-12}	1.99×10^{-04}	99.45	3.33×10^{-10}	1.31×10^{-05}	50.5
1048	2400	6.91×10^{-12}	2.07×10^{-04}	99.55	3.67×10^{-10}	2.01×10^{-05}	59.9
1053	2400	7.51×10^{-12}	2.19×10^{-04}	99.66	4.11×10^{-10}	3.15×10^{-05}	70.4
1073	2400	1.32×10^{-11}	2.53×10^{-04}	99.85	1.51×10^{-10}	3.71×10^{-05}	74.3
1088	2400	3.91×10^{-12}	2.73×10^{-04}	99.90	1.09×10^{-10}	4.17×10^{-05}	77.1
1103	2400	5.14×10^{-12}	3.36×10^{-04}	99.98	1.65×10^{-10}	5.01×10^{-05}	81.3
CO_2 laser extraction:		1.48×10^{-12}			8.36×10^{-10}		
Total:		6.95×10^{-09}			3.91×10^{-09}		

		^{40}Ar[d]			^{36}Ar[d]		
		Gas[a] (active blank)	D/a^2	F[b] (%)	Gas[a] (active blank)	D/a^2	F[b] (%)
1003	2400	5.57×10^{-12} (1.9×10^{-13})	7.06×10^{-09}*	1.4	1.79×10^{-14} (6.3×10^{-16})	9.3×10^{-09}*	1.60
1023	2400	8.45×10^{-12} (4.1×10^{-13})	3.73×10^{-08}*	3.2	2.73×10^{-14} (1.4×10^{-15})	4.2×10^{-08}*	3.38
1039	2400	1.45×10^{-11} (5.5×10^{-13})	1.50×10^{-07}*	6.3	4.8×10^{-14} (1.85×10^{-15})	1.6×10^{-07}*	6.52
1041	2400	3.55×10^{-11} (5.7×10^{-13})	7.61×10^{-07}	13.9	1.17×10^{-13} (1.9×10^{-15})	7.9×10^{-07}	14.16
1048	2400	1.90×10^{-11} (6.4×10^{-13})	1.30×10^{-06}	18.0	6.28×10^{-14} (2.1×10^{-15})	1.3×10^{-06}	18.25
1053	2400	3.04×10^{-11} (6.9×10^{-13})	2.52×10^{-06}	24.5	1.00×10^{-13} (2.3×10^{-15})	2.6×10^{-06}	24.78
1073	2400	7.50×10^{-12} (8.3×10^{-13})	2.89×10^{-06}	26.1	2.51×10^{-14} (2.7×10^{-15})	3.0×10^{-06}	26.42
1073	2400	4.19×10^{-12} (9.9×10^{-13})	3.11×10^{-06}	27.0	1.35×10^{-14} (3.3×10^{-15})	3.2×10^{-06}	27.30
1088	2400	1.13×10^{-11} (1.2×10^{-12})	3.76×10^{-06}	29.4	3.78×10^{-14} (3.4×10^{-15})	3.8×10^{-06}	29.76
1103	2400	2.02×10^{-11} (1.4×10^{-12})	5.10×10^{-06}	33.8	6.70×10^{-14} (4.8×10^{-15})	5.2×10^{-06}	34.13
1118	2400	1.27×10^{-11} (1.7×10^{-12})	6.08×10^{-06}	36.5	4.23×10^{-14} (5.7×10^{-15})	6.2×10^{-06}	36.89
CO_2 laser extraction:		2.96×10^{-10} ($<3 \times 10^{-15}$)			9.71×10^{-13}($<1 \times 10^{-17}$)		
Total:		4.66×10^{-10}			1.53×10^{-12}		

and $^{+}$ represent the Ar and He extraction time (s), respectively.

* Steps not included in Arrhenius fits due to the low fraction of gas released and the possibility that sample irregularities influenced the amount of gas extracted.

[a] Moles of gas extracted at each step (corrected for blanks). The helium, neon and argon extracted during the laser fusion step (after the step heating protocol) are given in the last row. The active blank is relevant only for the Ar data; it is considered to be negligible for the other noble gases: He ($<3 \times 10^{-15}$ mol) and Ne ($<7 \times 10^{-16}$ mol).

[b] Parameter F is the gas fraction released during each heating step. The gas fraction released during step i, F_i, is equal to C_i/C_{tot}, where C_i is the gas measured during step i and C_{tot} is the total amount of gas extracted ($=\sum C_i + C_{laser\ extraction}$).

[c] In the two data sets of glass G2, the sample is a single grain of radius $a = 1.075$ mm (mass = 12 mg).

[d] In the four data sets of glass G1, the sample is a single grain of radius $a = 0.35$ mm (mass = 0.55 mg).

[e] ^{4}He and ^{40}Ar were extracted by two successive step heating experiments: one for He (600s) and one for Ar (2400/1200s).

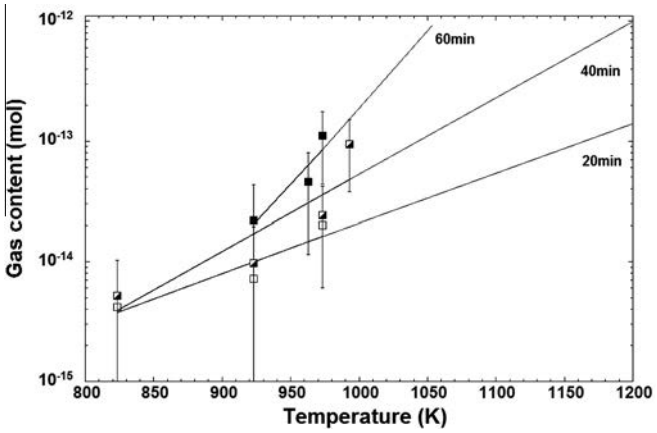


Fig. 1. Ar blanks as a function of temperature for three different accumulation times: 20 min, empty squares; 40 min, black and white squares; and 60 min, solid squares. Interpolation of these curves was used in order to calculate the blanks appropriate for each extraction (given in Table 1); errors of 100% were applied to the blank estimates.

de Paris, France. Temperature was measured with two Pt–Pt/Rh10% thermocouples placed at the top and the bottom of the cylinder. After 15 min at a given temperature (to ensure that the system was in thermodynamic equilibrium), the sample was submitted to a constant stress (σ), and its length (l) was measured as a function of time (t). Viscosity (η) can be calculated as (Neuville, 2006):

$$\eta = \frac{l * \sigma}{3\left(\frac{d\ln(l)}{dt}\right)}, \tag{2}$$

where η is in Pa s, σ in Pa, l in m, and t in s. A full description of the experimental apparatus and methods can be found in Neuville and Richet (1991) and Neuville (2006). The precision of the method is 0.02 $\log_{10}$ Pa s; a very low temperature gradient along the sample ($\sim$0.1 K) is critical to reach such a high precision. Viscosity measurements are given in Table 2 and plotted in Fig. 2 in an Angell plot (i.e. viscosity versus T_g/T). The glass transition temperature is the temperature at which the viscosity is equal to 10^{12} Pa s: thus we obtain $T_g = 1005$ K for glass G1. From Neuville (1992), it is possible to estimate that $T_g = 1080 \pm 20$ K for glass G2.

Table 2
Viscosity results for glass G1, measured using a creep apparatus (see text for further details).

Temperature (K)	1072.1	1060.1	1046.1	1036.4	1028.1	1025.9	1018.5	1015.5	1007.5	997.5
Log viscosity (Pa s)	8.97	9.55	10.05	10.49	10.84	10.97	11.38	11.47	11.88	12.42

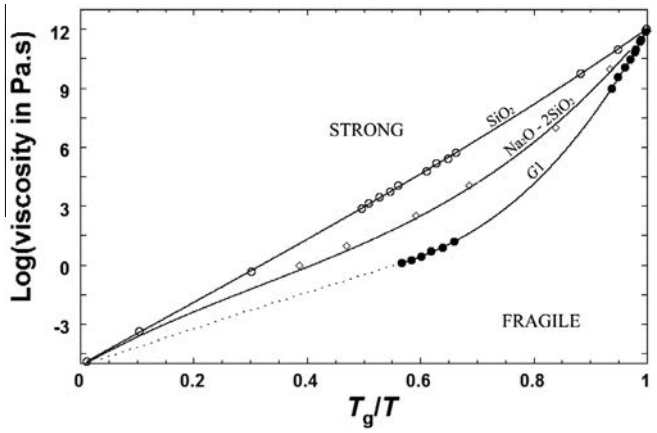


Fig. 2. Common logarithm of the viscosity η (Pa s) of composition G1 (solid circles) as a function of T_g/T (where T_g is the glass transition temperature). Literature data for SiO_2 (open circles) and Na_2O–$2SiO_2$ (open diamonds) are shown in order to illustrate fragile vs. strong behavior. The high T_g/T data for G1 were measured using a creep apparatus (this study; Table 2). The low T_g/T data for G1 are from Machin et al. (1952). A linear evolution of viscosity as a function of T_g/T is typical of "strong" liquids and glasses whereas concave-downward curves correspond to "fragile" melts and glasses and result from rupturing the silicate network.

3. NOBLE GAS RESULTS

3.1. Step heating experiments

Blank-corrected values of ^{4}He, ^{20}Ne, ^{36}Ar and ^{40}Ar in the step heating experiments are given in Table 1 for glasses G1 and G2. The gas fraction released from glass G1 is plotted as a function of temperature in Fig. 3: He is released at lower temperatures (mostly between 523 and 963 K) than Ne (for which gas release becomes significant only above 653 K; Table 1); there is almost no Ar release below 1000 K. These first order observations indicate that the smaller the size of the diffusing atom, the greater its diffusivity (at a given temperature): $D(\mathrm{He}) > D(\mathrm{Ne}) > D(\mathrm{Ar})$, where $D(\mathrm{He})$ is the diffusion coefficient of He, and so on. As a result of their slower diffusivities, not all of the Ne and Ar were extracted during the step heating protocol and some gas (18.7% for Ne and 66.2% for Ar) was extracted during the laser fusion step (Fig. 3).

The total concentrations of noble gases extracted from the glass fragments are relatively low: 9.3×10^{-7} mol g^{-1} (^{40}Ar), 3.0×10^{-9} mol g^{-1} (^{36}Ar), 7.8×10^{-6} mol g^{-1} (^{20}Ne) and 1.4×10^{-5} mol g^{-1} (^{4}He) for G1 and 2.2×10^{-6} mol g^{-1} (^{40}Ar) and 7.3×10^{-6} mol g^{-1} (^{4}He) for G2 (see Table 3). From the model published by Iacono et al. (2010), the noble gas solubilities at 1.2 GPa and 1760 K are estimated to be 9.1×10^{-5} mol g^{-1} for He, 3.1×10^{-5} mol g^{-1} for Ne, and 5.4×10^{-6} mol g^{-1} for Ar in glass G1 and 1.9×10^{-4} mol g^{-1} for He and 1.7×10^{-5} mol g^{-1} for Ar in glass G2. When the capsule was loaded with noble gases, the quantities of gases expected to be trapped into the sealed platinum capsule were $\sim 1.3 \times 10^{-5}$ (^{4}He), $\sim 2.6 \times 10^{-6}$ (^{20}Ne) and $\sim 8.6 \times 10^{-7}$ (^{40}Ar) moles (assuming a capsule length of 12.4 mm, an internal diameter of 2.6 mm and a pressure of the gas mixture of 3 bars). This is sufficient to saturate with noble gases the ~32 mg (G1) and 45 mg (G2) of glass loaded into the capsules (see Table 3). Thus the relatively

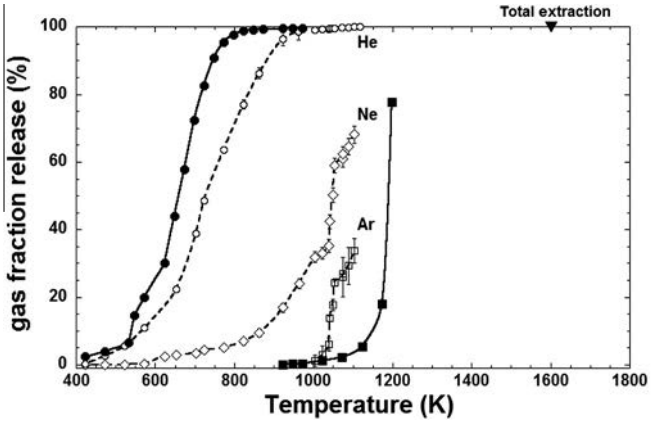


Fig. 3. He (circles), Ne (diamonds) and Ar (squares) release profiles for G1 (white) and G2 (black) glasses. Helium is completely degassed at the end of the step heating experiments while ~65% and ~20% of the Ar and Ne, respectively, remain trapped in the glass G1 (due to their lower diffusion rates). The remaining Ar and Ne were extracted by complete melting of the sample using a CO_2 laser in a separate experiment.

Table 3
Noble gas loss during the doping process of the G1 and G2 glasses.

		Solubility[a] mol/g	Gas capsule[b] mol/g	Gas glass[c] mol/g	Gas loss[d] %	Glass homogeneity[e] mol/g	mol/g	mol/g	%
G1	^{40}Ar	5.4×10^{-6}	2.7×10^{-5}	9.3×10^{-7}	−96.6	–	–	–	–
	^{20}Ne	3.1×10^{-5}	8.1×10^{-5}	7.8×10^{-6}	−90.4	–	–	–	–
	^{4}He	9.1×10^{-5}	2.9×10^{-4}	1.4×10^{-5}	−95.2	–	–	–	–
G2	^{40}Ar	1.7×10^{-5}	1.9×10^{-5}	2.2×10^{-6}	−88.5	1.9×10^{-6}	1.8×10^{-6}	2.0×10^{-6}	7%
	^{4}He	1.9×10^{-4}	2.9×10^{-4}	7.3×10^{-6}	−97.5	1.3×10^{-5}	1.2×10^{-5}	1.1×10^{-5}	9%

[a] The solubility of noble gases at the P–T conditions of the piston-cylinder experiments (1.2 GPa–1760 K) was computed using the model of Iacono et al. (2010).

[b] Quantities of noble gases loaded in the capsule (number of moles of noble gases loaded in the capsule divided by the mass of glass powder). The number of moles of noble gases was computed assuming a capsule length of 12.4 mm, an internal diameter of 2.6 mm and a pressure of the gas mixture of 3 bars.

[c] Quantities of noble gases extracted from the glass fragments in the step heating experiments.

[d] Percentage of gas loss expressed as the ratio (Gas glass – Gas capsule)/Gas capsule. This gas loss presumably occurred when the capsules were crimped in a vice just before welding.

[e] Quantities of He and Ar extracted by laser fusion of 3 chips of glass G2 of 6.7×10^{-2}, 2.9×10^{-1} and 2.35×10^{-1} mg (columns 7 to 9, respectively). The variability (%, last column) is expressed as the ratio of the standard deviation divided by the average quantity of He or Ar extracted.

low concentrations of noble gases measured in the glass fragments suggest that a significant proportion of gas was lost (up to ~95% in average in glass G1, and 93% in glass G2) either before the sealing of the platinum capsules or during the piston-cylinder experiments (see Table 3). This does not affect, however, the diffusivity measurements as the noble gas contents in the glass fragments are large enough to overcome high temperature procedural blanks (see Table 1 and Fig. 1). The glass homogeneity was verified by laser fusion of 3 different aliquots of c. 6.7×10^{-2}, 2.9×10^{-1} and 2.35×10^{-1} mg of glass G2: the final glass exhibits reasonably homogeneous noble gas concentrations with <7% variability in Ar concentrations and <9% variability in He concentration.

The large diffusion coefficients of He, and to a lesser extent Ne, in silicate glasses suggest that some of the noble gases in our glass fragments could be lost at room temperature by diffusion during the ~ two weeks between the end of the piston-cylinder experiments and the beginning of the step heating experiments. This would mean that the initial distribution of noble gases in the glasses was not uniform and therefore that we cannot use the expressions from Fechtig and Kalbitzer (1966). If we extrapolate our experimental data to 298 K (the approximate storage temperature of our glasses), we obtain normalized diffusion coefficients, D/a^2, equal to 5.05×10^{-14} s^{-1} for He and 1.17×10^{-14} s^{-1} for Ne. The percentage of noble gases lost from a spherical fragment over a time interval Δt can be estimated using the function:

$$f = 6\sqrt{\frac{\frac{\Delta t D}{a^2}}{\pi}} - 3\Delta t\frac{D}{a^2} \quad (3)$$

where f is the fractional gas loss (Crank, 1975). For a time interval of two weeks at 298 K, we calculate diffusional losses of 0.08% for He and 0.04% for Ne, which can be considered as negligible for our application. This result is confirmed by isothermal steps of 20 min at room temperature performed for blank purpose: the blank values were negligible for both He and Ne (under a high vacuum of 10^{-8} mbar). Therefore, we can reasonably assume that no significant diffusional loss happened between the end of the piston-cylinder experiments and the beginning of the step heating experiments.

3.2. Diffusion coefficients of noble gases

The diffusion coefficients measured for ^{4}He, ^{20}Ne, ^{36}Ar and ^{40}Ar are given in Table 1 and plotted as a function of $1/T$ in Fig. 4. The diffusivities of the noble gases in the glasses investigated do not display simple Arrhenian behavior: it is not possible to define a single slope and intercept for any of the gases in a plot of $\mathrm{Log}(D/a^2)$ vs. $1/T$ (Fig. 4). Nevertheless, there are distinct regions for each gas where $\mathrm{Log}(D/a^2)$ is a linear function of inverse temperature. These regions of "Arrhenian behavior" are separated by clear changes in slope. For both glasses, the first few diffusion measurements at low temperatures do not lie on the lines that best fit the diffusion data at higher temperatures or define trends that are difficult to reconcile with physical diffusion mechanisms. In some cases, these deviations are presumably due to the small gas fractions extracted during these low temperature steps: for instance, $F \leqslant 0.33\%$ for He and Ne in glass G1. In other cases, it seems likely that the first steps of noble gas release have been affected by the irregular shape of our sample grains. For example, the Ar diffusion data for glass G2 show a well-defined linear trend in the six lowest temperature steps (grey diamonds at 723–898 K; Fig. 4). The slope of this trend indicates, however, an activation energy of only 60 kJ mol^{-1}, which is very low in comparison to the activation energy measured at $T > 923$ K of 166 kJ mol^{-1}. Accordingly, we presume that it is not representative of Ar diffusion in glass, and that it is biased by preferential gas extraction from shards and spines in our irregular samples. Such shape effect leads to anomalously high diffusivities as the average diffusion distance is significantly shorter (and the fractional loss is greater) than in the case of a sphere (Eq. 1a–c). The first diffusion measurement for He in glass G2 seems also slightly

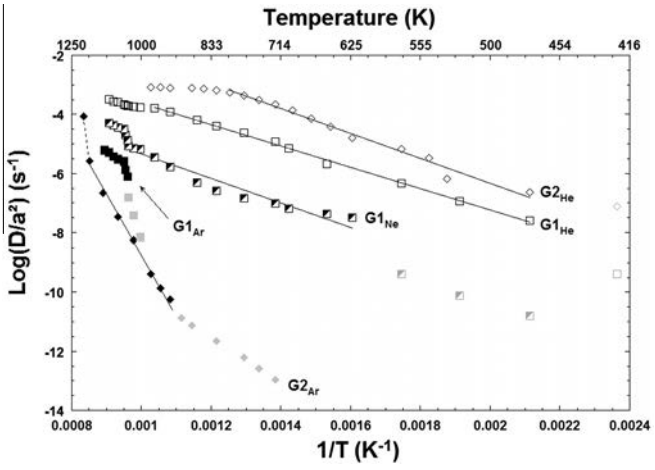


Fig. 4. Diffusion coefficients of ^{4}He, ^{20}Ne and ^{40}Ar in glasses G1 and G2. Symbols are as follows: squares and diamonds for G1 and G2, respectively; ^{4}He empty, ^{20}Ne half-filled and ^{40}Ar filled. The grey symbols are not included in the fit for determining the low temperature Arrhenius parameters (see text for an explanation).

overestimated and could be affected by this shape effect. The shape effect is expected to be limited to the lowest temperature steps because shards and spines should rapidly get depleted in noble gases. Similar phenomena have been reported in Ar diffusion studies in glasses and minerals (Fechtig and Kalbitzer, 1966; McDougall and Harrison, 1999). It is therefore justifiable to ignore the first few release steps of each sample. The steps ignored are indicated by stars in Table 1 and by grey symbols in Fig. 4.

There was almost no Ar released from glass G1 at $T < T_g$, so our diffusion data in this glass are at $T \sim T_g$ and above. The diffusion data for the three lowest temperature steps exhibit a well-defined linear trend (grey squares at 1003–1039 K; Fig. 4). The slope of this trend yields, however, a value of ~350 kJ mol^{-1}, which is unreasonably high for an activation energy: for comparison, the activation energy for Si diffusion in amorphous silica is 255 kJ mol^{-1} (Brebec et al., 1980). This behavior is opposite to that observed in glass G2 and cannot be due to the shape effect. The high activation energy inferred for glass G1 at low temperature seems unlikely to correspond to Ar diffusion through the melt ($T > T_g$) but may reflect some softening processes affecting the glass structure at $T \sim T_g$ (see Section 4.3). This assumption seems to be confirmed by the similarity with the Ne diffusion behavior at $T \sim T_g$. However, these observations are only made on three temperature steps and we would need data at lower temperatures ($T < T_g$) to demonstrate a non-Arrhenian behavior of Ar close to the glass transition temperature. At this point, we consider that our low-T database for Ar is too limited to fully explain an activation energy as high as 350 kJ mol^{-1}. For this reason, we have decided to exclude the three lowest temperature steps in our database ($T = 1003$, 1023 and 1039 K), although the fractions released for these temperatures are not negligible ($F = 1.4\%$, 3.2% and 6.3%, respectively). Further experiment, at lower temperature ($T < T_g$) are required to confirm the non-Arrhenian behavior for Ar at $T \sim T_g$.

The Ne diffusion data for glass G1 clearly show two distinct behaviors (ignoring the anomalous low temperature points). Between 623 and 863 K, there is a well-defined linear region, followed by a non-linear region which asymptotically tends to a straight line with increasing temperature (Fig. 4). It is significant that this deviation from linearity occurs close to the T_g computed from the viscosity measurements. The He diffusivity data for both glasses (G1 and G2) display a similar non-linearity (i.e. a low temperature linear region followed by a curved region), although no diffusive jumps are observed, in comparison to that of Ne. The He diffusion data seems therefore to quickly reach a

Table 4
Parameters T_2, A_1/a^2, B_1 and C estimated by fitting the modified VTF relationship (Eq. (6)) and Arrhenius law (Eq. (4)) to our He, Ne and Ar diffusion data for G1 and G2 glasses.

G1	Regime [1]	T_2 (K)	A_1/a^2 (s^{-1})	B_1 (kJ mol^{-1})	C (kJ.mol^{-1})
Ar	Glass	–	–	–	–
	T_g transition	–	–	–	–
	HT (10411118 K)	–	$2.3 \times 10^2 \pm 40$	–	98.5 ± 17
Ne	Glass (653–1023 K)	–	0.97 ± 0.02	–	34.5 ± 2.85
	T_g transition (1039–1103 K)	1034.4	2.6×10^{-2}	0.06	56.7
	HT	–	–	–	–
He	Glass (473–823 K)	–	$6.4 \times 10^{-2} \pm 2.7 \times 10^{-2}$	–	30 ± 0.45
	T_g transition (863–1023 K)	790	7.55×10^{-3}	3.1	18.8
	HT	–	–	–	–
G2	Regime [1]	T_2 (K)	A_1/a^2 (s^{-1})	B_1 (kJ mol^{-1})	C (kJ mol^{-1})
Ar	Glass (923–1073 K)	–	$1.8 \times 10^{11} \pm 3.27 \times 10^9$	–	166 ± 4.6
	T_g transition	–	–	–	–
	HT	–	–	–	–
He	Glass (533–748 K)	–	$1.2 \times 10^2 \pm 9$	–	35 ± 2.25
	T_g transition [2] (773–973 K)	750	1.5×10^{-3}	0.27	3.8
	HT	–	–	–	–

[1] For each gas, three different regimes are distinguished: glass regime, T_g transition, and high temperature domain (HT; see text for discussion). In the glass regime, the diffusion behavior is Arrhenian, and A_1/a^2 and C are equivalent to D_0/a^2 and E_a respectively (and $B_1 = 0$).
[2] Although T_g has not been measured for glass G2, the curve fitted in order to estimate these T_2, A_1/a^2, B_1 and C parameters likely encompasses the T_g (see Fig. 8).

plateau. Also, the temperatures at which the diffusion regime switches from linear to non-linear are not the same for He and Ne. The linear portions of the Arrhenius diagrams (Fig. 4) can be interpreted as temperature activated diffusion through the glass structures. The He and Ne activation energies in G1 are slightly different with E_a(He) $= 30 \pm 0.45$ kJ mol^{-1} and E_a(Ne) $= 34.5 \pm 2.85$ kJ mol^{-1} (Table 4).

Diffusion of ^{4}He in glass G2 is similar to that observed in glass G1: a linear correlation between $\log(D/a^2)$ and $1/T$ from 473 to 798 K, corresponding to an Arrhenian behavior with $E_a = 35 \pm 2.25$ kJ mol^{-1}. This is followed by a non-Arrhenian regime at higher temperatures (Table 4). As discussed above, diffusion of ^{40}Ar for the six extraction steps between 723 and 898 K in glass G2 defines a linear correlation corresponding to an activation energy $E_a = 64.5$ kJ mol^{-1}. However, the gas fractions released at these temperatures are very low ($F < 0.1\%$; Table 1) so these data are presumably biased by gas release from the sample surface irregularities. At $T > 898$ K, ^{40}Ar diffusion shows a linear behavior corresponding to an activation energy $E_a = 166 \pm 4.6$ kJ mol^{-1}, which is close to that expected for Ar diffusion in a silicate glass or liquid. For comparison, E_a equals 133 ± 24 kJ mol^{-1} in albite (Na_2O-Al_2O_3-SiO_2) glass (Roselieb et al., 1992) and 175.7 kJ mol^{-1} in a K_2O-CaO-Al_2O_3-SiO_2 glass (Reynolds, 1957).

3.3. Diffusion coefficients of Ar isotopes

Our step heating experiments demonstrate that the two isotopes of Ar do not diffuse at the same rate, with ^{36}Ar diffusing more rapidly than ^{40}Ar. In a plot of the ratio D(^{40}Ar)/D(^{36}Ar) as a function of T (Fig. 5), the diffusion of ^{40}Ar is less than 3% slower than that of ^{36}Ar at high temperatures ($T > 1040$ K), with D(^{40}Ar)/D(^{36}Ar) equal to 0.98 ± 0.14. The three data at the lowest temperatures suggest that D(^{40}Ar)/D(^{36}Ar) may become strongly temperature sensitive at temperatures close to the glass transition: at 1003 K, the diffusion of ^{40}Ar is 24% slower than that of ^{36}Ar. At present, we don't know if this strong kinetic fractionation of Ar isotopes at low temperatures is due to structural changes close to the glass transition or if it is an experimental artifact related, for instance, to the small fractions of noble gases extracted at these temperatures. Replicate experiments are needed to confirm the strong kinetic fractionation of ^{36}Ar and ^{40}Ar close to the transition temperature.

4. DISCUSSION

4.1. Relationship between diffusion coefficient and temperature: alternatives to the Arrhenius law

It is commonly established that transport properties strongly depend on temperature. The relationship between diffusion coefficient, D (and therefore the D/a^2 parameter) and temperature, T, is described by the Arrhenius equation:

$$\frac{D}{a^2} = \frac{D_0}{a^2} e^{-E_a/(RT)} \quad (4)$$

where D_0 is the pre-exponential term, corresponding to an limiting diffusivity at $T = \infty$, E_a is the activation energy for diffusion (J mol^{-1}), R the gas constant (=8.314 J K^{-1} mol^{-1}) and a is the diffusion domain radius (taken to be the sample size in our case). Thermally activated diffusion thus results in a straight line in a plot of Log(D/a^2) versus $1/T$. Nonetheless, it has been shown that diffusion in glass can diverge from the classical Arrhenius equation, particularly at temperatures close to or above T_g (Braedt and Frischat, 1988; Behrens, 1992). Different relationships (principally empirical) have been derived to account for the departures from Arrhenian diffusion at T close to T_g. The empirical VTF equation (Vogel, 1921; Fulcher, 1925; Tammann and Hesse, 1926), originally established to describe the viscosity temperature dependence of molten silicate, has been adapted to account for ionic conductivities σ (Caillot et al., 1994):

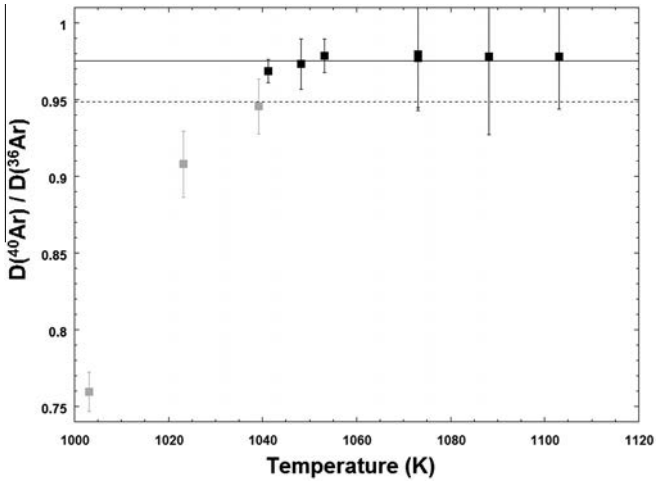


Fig. 5. Relative ^{40}Ar-^{36}Ar diffusivities in glass G1 as a function of temperature. The dashed line corresponds to Graham's law: D(^{40}Ar)/D(^{36}Ar) = 0.95. The solid line corresponds to the average value of the high temperature data (solid symbols; $T > 1040$ K): D(^{40}Ar)/D(^{36}Ar) $= 0.98 \pm 0.14$ (2-σ).

$$\sigma = A * \exp\left(-\frac{B}{R(T - T_2)}\right) \quad (5)$$

The variable B can be interpreted in terms of a "pseudo-activation energy" associated with diffusive jumps facilitated by structural rearrangements (Caillot et al., 1994; Russell et al., 2003). T_2 is the temperature at which the diffusion regime switches from Arrhenian to non-Arrhenian and is thereafter referred to as the switch temperature; A is equivalent to the pre-exponential factor of Arrhenius equation. Macedo and Litovitz (1965) developed a modified VTF relationship, which combines an Arrhenius-like term with the VTF parameterization. Miyamoto and Shibata (1973) and Cheradame (1982) used this modified VTF relationship to better fit their conductivity data on salt-polymer complexes at high temperature. We propose here to use the modified VTF equation in order to explain the diffusion behavior of noble gases in our glasses:

$$\frac{D}{a^2} = \frac{A_1}{a^2} * \exp\left(-\frac{B_1}{R(T - T_2)} - \frac{C}{RT}\right) \quad (6)$$

The variables A_1 is equivalent to A in Eq. (5) and C is equivalent to the activation energy of an Arrhenius equation. B_1, similar to the variable B, can be also interpreted as a "pseudo-activation energy" that reflects the influence of the silicate network relaxation on the diffusant in question. When B_1 tends to 0, Eq. (6) tends to a classical Arrhenius equation implying that diffusion is a simple thermally activated process. Therefore, when $B_1 = 0$, diffusive jumps are constrained by a fixed energy barrier between the diffusive sites within the silicate network.

Diffusion through a glass can be considered as successive jumps between free volume sites in the silicate network (Doolittle, 1951; Turnbull and Cohen, 1961, 1970; Williams et al., 1955; Cohen and Grest, 1979), and the availability of the free volumes determines the diffusive behavior of a species. When $B_1 \neq 0$ (i.e. non-Arrhenian behavior), there is an additional probability of an interstitial atom accessing newly created free volume due to enhanced mobility of atoms within the silicate network (i.e. available site distribution varies due to modifications in the distribution of free volume within the silicate network). Note that parameters A_1, A, B, B_1 and T_2 obtained by fitting the experimental data have different physical significance depending on the microscopic model chosen to describe the diffusion mechanisms.

Non-Arrhenian behavior is observed in glass G1 as T_g is approached (Fig. 4). It is characterized by an upward curvature, stronger for heavy noble gases (Ne, Ar) than for He (Fig. 4). This upwards curvature can be related to the lattice mobility which allows the diffusing atoms to move faster within the silicate network. As a consequence, the diffusion coefficient increases because the free volume (available site for diffusive jumps) increases. However, a plateau is reached as soon as the lattice mobility stops being critical for the atoms diffusion jumps. This stage is feasible when the distance between two sites is large enough to not affect the noble gas diffusive jump within the silicate network. Therefore, atoms of different sizes will be affected differently as a function of their ease to jump from one site to another. Smaller atoms (He) will be less affected than larger atoms (Ne) (Fig 4). The switch from an Arrhenian to a non-Arrhenian diffusive regime occurs at different temperatures T_2 for the different gases. In order to quantify the different diffusive regimes (Arrhenian or non-Arrhenian) for He, Ne, and Ar in glasses G1 and G2, we fitted Eq. (6) to the data by least squares fitting. Solutions to Eq. (6) are not unique and the fitting procedure can yield physically nonsensical values for A_1/a^2, B_1, C and T_2 depending on the initial values assigned to those parameters. Nevertheless, by restricting the outputs to physically meaningful values, given by the initial fitting conditions, the solution of

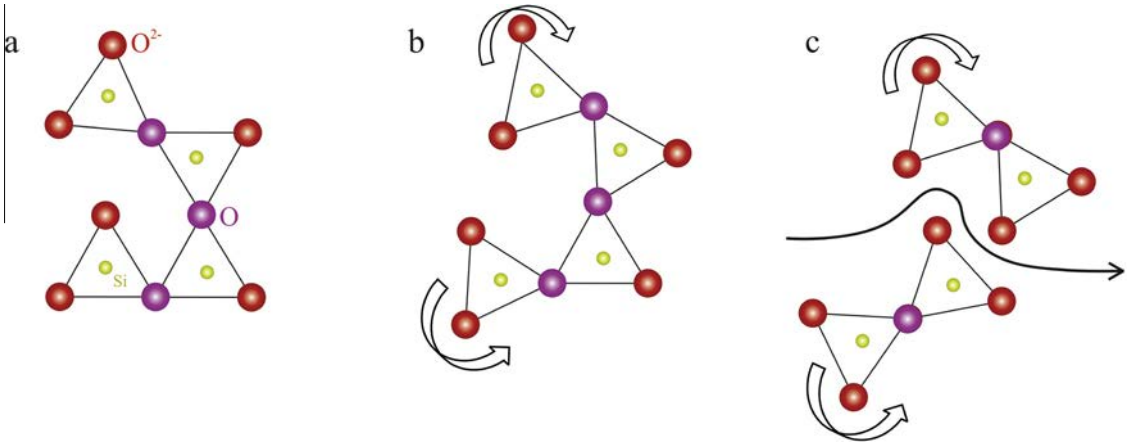


Fig. 6. 2D sketches illustrating the interactions between the non-bridging oxygens (O^{2-}, red circles) and the bridging oxygens (O, purple circles) within the glassy state (a), close to the glass transition (b), and in the melt (c). The yellow circles are Si atoms. In the glass (a), the spatial position of tetrahedral chains remains fixed. Diffusion of noble gases is therefore Arrhenian, and the free volume is constant. As the T_g is approached (b), thermal energy allows spatial modifications of the tetrahedra network (rotation, relative movement of tetrahedra, etc.) over short and medium range (double arrow line). The free volume is no longer fixed, and structural modifications enhance noble gas diffusion to a variable extent (large for Ne, small for He). In the liquid state ($T \gg T_g$) (c), energy is sufficient to break connection between two tetrahedral units and allow new diffusion pathways within the silicate network (thick arrow). The system is now dynamics, with oxygen exchange (bridging oxygen to non-bridging oxygens) under thermal excitation.

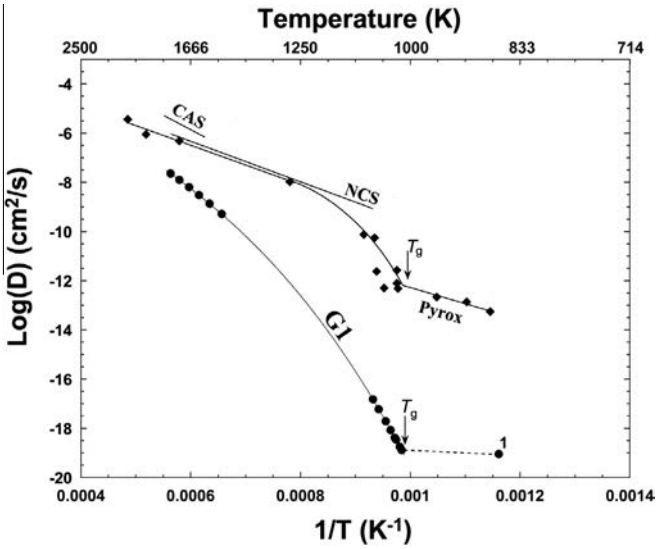


Fig. 7. Diffusion coefficients for O^{2-} (ionic oxygen) in G1 glass (solid circles; calculated from the viscosity data using Stokes–Einstein equation) and in several representative glass and melt compositions: CAS ($16CaO\text{-}12Al_2O_3\text{-}72SiO_2$) Oishi et al. (1975); NCS ($16Na_2O\text{-}12CaO\text{-}72SiO2$) Terrai and Oishi (1977); Pyrox ($53SiO_2\text{-}20CaO\text{-}14MgO\text{-}13FeO$), solid diamonds Magnien et al. (2008). The datum for G1 at $T < T_g$ (labeled 1) indicates the theoretical O^{2-} diffusion coefficient calculated from the minimum diffusion distance of the silicate network: ~150 pm (O–O bound length). Such an O^{2-} diffusion coefficient ($D = 9.4 \times 10^{-20}$ cm s^{-1}) at $T = 863$ K allows non-arrhenian behavior for He (see text for discussion).

Eq. (6) converges systematically towards the parameter sets listed in Table 4. Therefore, we observe a shift of the Arrhenian to non-Arrhenian switch temperature as a function of noble gas: $T_{2(He)} < T_{2(Ne)}$ where $T_{2(He)} = 863$ K and $T_{2(Ne)} = 1034.4$ K are the switch temperatures of He and Ne respectively. A switch temperature for Ar cannot be calculated due to the lack of data at temperatures below T_g.

The reason why similar non-Arrhenian diffusion profiles have not been observed for noble gases in the past may be that most diffusion measurements were made in silica-rich glasses. This is emphasized by Ar diffusion in glass G2, which is a silica-rich glass compared to G1 and which shows a well-defined Arrhenius profile (Fig 7c; Ar data are not available for glass G1 in this temperature range).

4.2. Glass structure: a microscopic view

As discussed previously, the silicate network strongly influences diffusion of the noble gases over the temperature range investigated. It is therefore necessary to understand the glass structure in order to determine how it controls diffusion processes in glasses.

It is well known that in silicate glasses Si^{4+} is a network former while Ca^{2+}, Na^{+}, K^{+} and $Mg^{2}+$ act as network modifiers or charge compensators as a function of the ratio $M^{x+}_{2/x}O/Al_2O_3$ (M = Mg, Ca, Na, K). The addition of modifier cations to silica glass depolymerizes the Si–O–Si glass network by breaking Si–O bonds and forming non-bridging oxygens (NBO; see Le Losq et al. (2014) for a detailed explanation). Binary $M^{x+}_{2/x}O$–SiO_2 glass mixtures have short-range order (for instance, a SiO_2 tetrahedron) and medium-range order (e.g. chains of tetrahedra which lead to ordering up to about 1 nm), but they lack the long-range order and symmetry of crystals (Parks and Huffman, 1928; Doremus, 1975). Diffusion of inert tracers through the glass or (incipient) liquid will be extremely sensitive to rearrangement of the glass structure at short and medium length scales.

4.3. Silicate glass structure and noble gas diffusion

Increasing temperature leads to the creation of additional potential host sites (available empty space within the glass structure) for the noble gases, and thus to faster diffusion (Chakraborty, 1995). Our diffusion data (Fig. 4) can be explained by modifications of the silicate network (i.e. free volume variation) as the temperature approaches T_g. Therefore, the kinetics of the silicate network modification needs to be probed in order to identify potential diffusion pathways of each noble gas within the glass medium. As the structure of the silicate network is controlled by bulk composition, it is also expected that the number of host sites created with increasing temperature varies with the glass/melt composition. As a consequence, light (He) and heavier (Ar) noble gas diffusivities in silica-rich glasses compared to depolymerized glasses should reflect the effect of glass structure. A microchannel model is presented in order to explain He and Ar diffusion data in G1 and G2 glasses.

4.3.1. Silicate tetrahedra rupture: The O^{2-} diffusion probe

Ionic oxygen diffusion is principally related to diffusion of non-bridging oxygens within the glass structure and can be used as a probe for investigating the rate of modification of the silicate network (Oishi et al., 1975; Dunn, 1982). Free oxygen ions are either able to diffuse through the network without impacting the arrangement of silica tetrahedra within the melt (Sasabe and Goto, 1974; Wendlandt, 1980) or else O^{2-} diffusion is limited by

translational and/or rotational movement of the SiO_4 tetrahedral units requiring that Si[Al]–O bonds are ruptured prior to O^{2-} displacement (Koros and King, 1962; Muehlenbachs and Kushiro, 1974). While bridging oxygens could also contribute to O^{2-} diffusion (for example through changes in coordination of oxygens within the tetrahedra), this is likely minor relative to the diffusion of non-bridging oxygens in the network. The different mechanisms involved result in different activation energies for O^{2-} diffusion: typically, low E_a^{O2-} are associated with free ionic displacement without displacement of the SiO_4 tetrahedra (Fig. 6a). From the literature, low E_a^{O2-} recorded in silicate melts are generally between ~100 and ~250 kJ mol^{-1} for natural tholeiitic basalt and andesite glasses (Wendlandt, 1980) and in synthetic glasses (May et al., 1974; Oishi et al., 1975; De Berg and Lauder, 1980; Dunn, 1982). Conversely, high values of E_a^{O2-} (>320 kJ mol^{-1}) have been measured in synthetic melts (Koros and King, 1962) and in natural basaltic melts (Muehlenbachs and Kushiro, 1974) and are associated with interactions between the O^{2-} and bridging oxygen bonds (Si–O or Al–O; Fig. 6c).

In order to evaluate whether displacements of non-bridging oxygen ions can affect glass structure and thus noble gas diffusion over the durations of our experiments, we need to have estimates of the relevant O^{2-} diffusion coefficients. These coefficients were computed for glass G1 at temperatures above T_g using the available viscosity data (Fig. 2) and Stokes–Einstein relation (Tarjus and Kivelson, 1995; Geyer et al., 1996):

$$D = \frac{kT}{6\pi\eta r} \tag{7}$$

where k is the Boltzmann constant (1.38×10^{-23} J K^{-1}), and r (m) is the effective molecular radius (Fig. 7). By setting r equal to the O–O bond length (1.485×10^{-10} m; Strausser et al., 2007), it has been shown that there is a good agreement between the diffusion coefficients calculated from viscosity measurements using Eq. (7) and independent determinations of O^{2-} diffusion (Oishi et al., 1975; Terrai and Oishi, 1977; Yinnon and Cooper, 1980). The O^{2-} diffusion coefficients calculated using Eq. (7) are plotted in Fig. 8. For comparison, O^{2-} diffusion data from the literature are also shown for different melt composition: CAS (CaO-Al_2O_3-SiO_2) (Oishi et al., 1975); NCS (Na_2O-CaO-SiO_2) (Terrai and Oishi, 1977) and Pyrox (SiO_2-CaO-MgO-FeO) (Magnien et al., 2008).

The activation energy at high T in glass G1 ($T > 1773$ K), E_a^{O2-}, is 337 kJ mol^{-1}. This is consistent with the higher values reported in the literature, and it indicates that the displacement of O^{2-} ions involves rupturing of Si[Al]–O bonds within the melt structure. At lower temperatures, between T_g and ~1300 K, we observe a strong increase in activation energy: $E_a = 764$ kJ mol^{-1} (Fig. 7). This high activation energy can be related to the increasing rigidity of the silicate network as the glass transition is approached. Thus, O^{2-} diffusion in glass G1 involves Si[Al]–O bond rupture both close to T_g and in the liquid state. The O^{2-} diffusion mechanisms in glass G1 at $T < T_g$ remain unknown, however, because we do not have measurements of E_a^{O2-} below T_g.

4.3.2. Time and length scales of free volume modification during the noble gas diffusion experiment

In both glasses investigated, He, Ne and Ar show Arrhenius behavior at low temperatures, corresponding to temperature activated diffusion through an immobile glass structure: the available free volume for diffusive jumps is static with respect to the possible diffusion mechanisms already described above.

If the non-Arrhenian behavior of He and Ne diffusion is related to modification of the silicate network, then this will only be possible if the network is sufficiently mobile to modify its free volume over the time scale of a diffusion experiment (typically 2400 s). Using the O^{2-} diffusivities estimated above for $T > T_g$, we can calculate characteristic O^{2-} diffusion distances: $x \approx [D(O^{2-})\cdot t]^{1/2}$. These diffusion distances need to be larger than interatomic distances in order to modify the network and create additional free volume for noble gas diffusion. We could make these calculations only for Ne because it switches to a non-Arrhenian diffusion regime at $T > T_g$. The switch to non-Arrhenian Ne behavior (at temperatures close to 1039 K) corresponds to O^{2-} diffusivities of 5×10^{-17} cm^2 s^{-1} and to O^{2-} diffusion distances of $\sim 500 \times 10^{-12}$ m (500 pm). These diffusion length scales are 2 to 3 times larger than Si-O (163 pm), Si-Si (233 pm), and O–O (148 pm) bond lengths (Strausser et al., 2007): it seems plausible therefore that there are some modifications to free volume at these temperatures and on these time scales. Noble gas diffusion at 1039 K is no longer simple temperature activated diffusion but is instead enhanced by simultaneous rearrangement of the silicate network. Similar structural changes have been invoked to explain non-Arrhenius behavior of Na diffusion in plagioclase glasses. In the case of Na self-diffusion in glass, Behrens (1992) attributes the change in slope to different relaxation processes close to T_g.

4.3.3. Silicate network mobility below the glass transition temperature

Our observations show, for the first time, the influence of free volume relaxation at temperatures well below T_g: 142 K lower than the experimentally determined T_g in the case of He diffusion through G1 glass. This indicates that the noble gases, particularly He, are extremely sensitive to the first slight modifications of the silicate network as T_g is approached. Also, these observations show that atomic radius influences the sensitivity of the noble gases to structural modifications within the silicate network, He reacting to structural modifications at lower temperatures than Ne.

As our viscosity measurements and O^{2-} diffusivity estimates are only available for $T > 997$ K, it is not possible to directly estimate network diffusion length scales at the temperature at which the He diffusion regime switches from Arrhenian to non-Arrhenian. Instead, we estimate the minimum O^{2-} diffusion coefficient needed in order to allow structural modifications over the time scale of the diffusion experiment, thus resulting in the non-Arrhenian He diffusion behavior observed. For this calculation, we considered a temperature corresponding at the onset of the non-Arrhenian regime for He diffusion ($T = 863$ K).

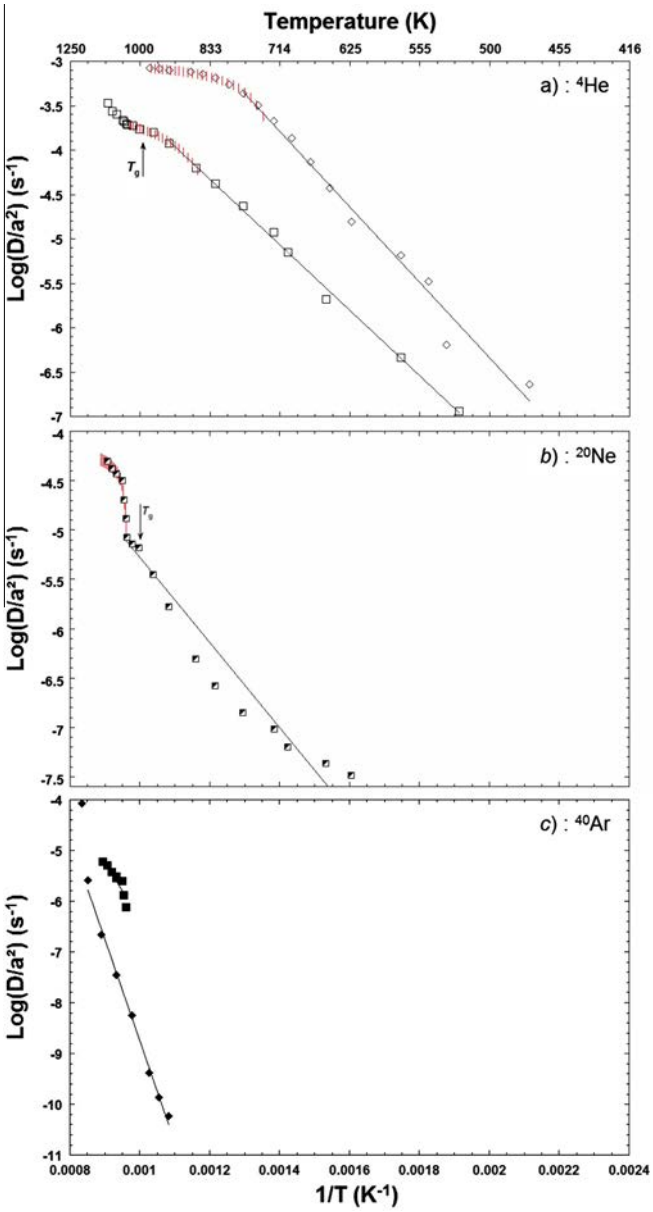


Fig. 8. Modified VTF and Arrhenian fits to the noble gas diffusion data: squares and diamonds correspond to the G1 and G2 experimental data, respectively. (a) ^{4}He; (b): ^{20}Ne and (c): ^{40}Ar. Noble gases show an Arrhenius behavior at low temperature, corresponding to diffusion in the pure glass structure (data are not available for Ar in G1 at low temperature). With increasing temperature, this is followed by non-Arrhenian segments (He, Ne) that are modeled using a modified VTF relation (Eq. (6) in the text). The error bars are smaller than the symbol sizes.

The O^{2-} diffusion distances need to be greater than characteristic interatomic distances of the silicate network (the O–O bond length of 148 pm) at $T = 863$ K. The minimum O^{2-} diffusivity that would permit structural rearrangements of the silicate network is of the order 1×10^{-19} cm^2 s^{-1}. The extrapolation of the O^{2-} diffusion trend to temperatures below T_g suggests much lower O^{2-} diffusivities at these temperatures (see Fig. 7). Nevertheless, Magnien et al. (2008) investigated O^{2-} diffusion in a Pyrox glass ($53SiO_2$-20CaO-14MgO-13FeO) at temperatures below the glass transition (Fig. 7). Their results show that at and below T_g, the O^{2-} activation energy is considerably lower. As a result, the O^{2-} diffusion coefficient varies little at $T < T_g$. It can be reasonably considered that a similar change in slope occurs in G1 glass. It seems plausible therefore that the O^{2-} diffusion distances could be sufficiently high to allow structural modifications in G1 at temperatures 142 K below T_g.

4.3.4. The effect of microchannels in the glass structure on noble gas diffusivities

While it has been established that He diffuses more rapidly in silica-rich glasses relative to depolymerized, silica-poor glasses (Shelby, 1974; Shelby and Eagan, 1976;

Behrens, 2010), our Ar diffusion data in G1 and G2 glasses show the opposite trend, i.e. Ar diffuses faster in silica-poor glass than in silica-rich glass. This observation is consistent with the study of Reynolds (1957) who obtained a similar relation between He and Ar diffusion in alkali silicate glasses (Fig. 9).

The presence of constrictions within the network is expected to impede diffusion of large noble gas atoms to a greater degree than smaller noble gas atoms. On the contrary, the presence of large and open diffusive pathways would allow all noble gases to diffuse at the same rate. Variations in D(He)/D(Ar) as a function of glass composition will therefore reflect the distribution of such restrictions in the glass network.

Greaves et al. (1981), see also (Greaves, 1985, 1989) suggested in the Modified Random Network (MRN) model that, in silicate glasses, alkali metals are concentrated in a local fine structure, known as microchannels, through the infinite disordered silicate network. This concept has since been corroborated by diffusion data (Greaves and Ngaï, 1995), imaging of the glass nanostructure (Frischat et al., 2004) and inelastic neutron scattering and molecular dynamic simulation (Meyer et al., 2005; Kargl and Meyer, 2008). The MRN model considers alkalis as network modifiers, and hence, the microchannels walls concentrate NBOs. Therefore, increasing the silica concentration tends to decrease the fraction of such channels constructed by the network-modifiers. On the other hand, this increase in silica leads to a more interconnected tetrahedral network, with an increase of the free volumes at the center of interconnected tetrahedral rings and cages (i.e. ring connectivity). It has also been recently shown by Le Losq et al. (2014) that aluminum excess contributes to creating connected tetrahedra in peraluminous high silica-glasses which also results in microchannels (Le Losq and Neuville, 2013).

Microchannels associated with large, strongly interconnected tetrahedral cages and rings in silica-rich glasses are likely to produce fast pathways for diffusion of specific noble gases that have atomic radii sufficiently small to pass through the channels. In contrast, poorly connected networks where the channels are occupied by network modifier cations probably do not represent diffusive pathways for the noble gases. As a result, diffusion in silica-poor glasses (which will also be poor in connected channels) may in turn

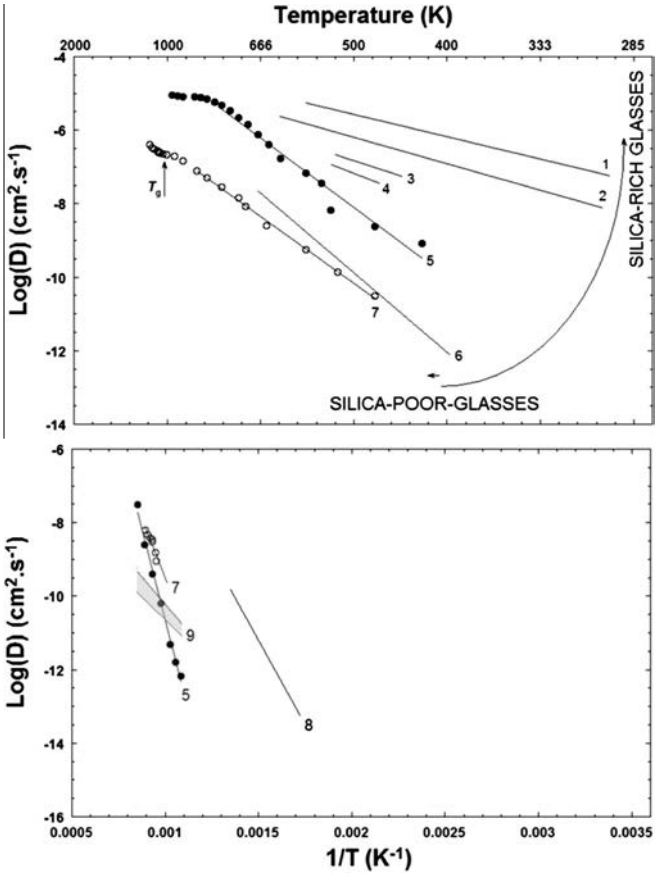


Fig. 9. Diffusion (D) of He (a) and Ar (b) in glasses of different chemical compositions. Only low pressure (0.1 MPa) measurements are shown. Data sources: 1: silica glass (SiO_2) Sweets et al. (1961); 2: Borosilicate ($81SiO_2$-$13B_2O_3$-$2Al_2O_3$-$4Na_2O$ wt%) Roger et al. (1954); 3: $0.5Na_2O$-$0.5Al_2O_3$-$3SiO_2$ (sodium aluminosilicate glasses) Shelby and Eagan (1976); 4: Na_2O-SiO_2 (NS3) glass Shelby and Eagan (1976); 5 and 7: G2 and G1 glasses respectively (this study); 6: natural MORB Kurz and Jenkins (1981); 8: potash-lime-silica-alumina glass ($62SiO_2$-$26K_2O$-$5CaO$-$5Al_2O_3$ mol%) Reynolds (1957) and 9: silica glass Perkins and Begeal (1971) and Nakayama and Shackelford (1990). He diffusivities are enhanced in silica-rich glass.

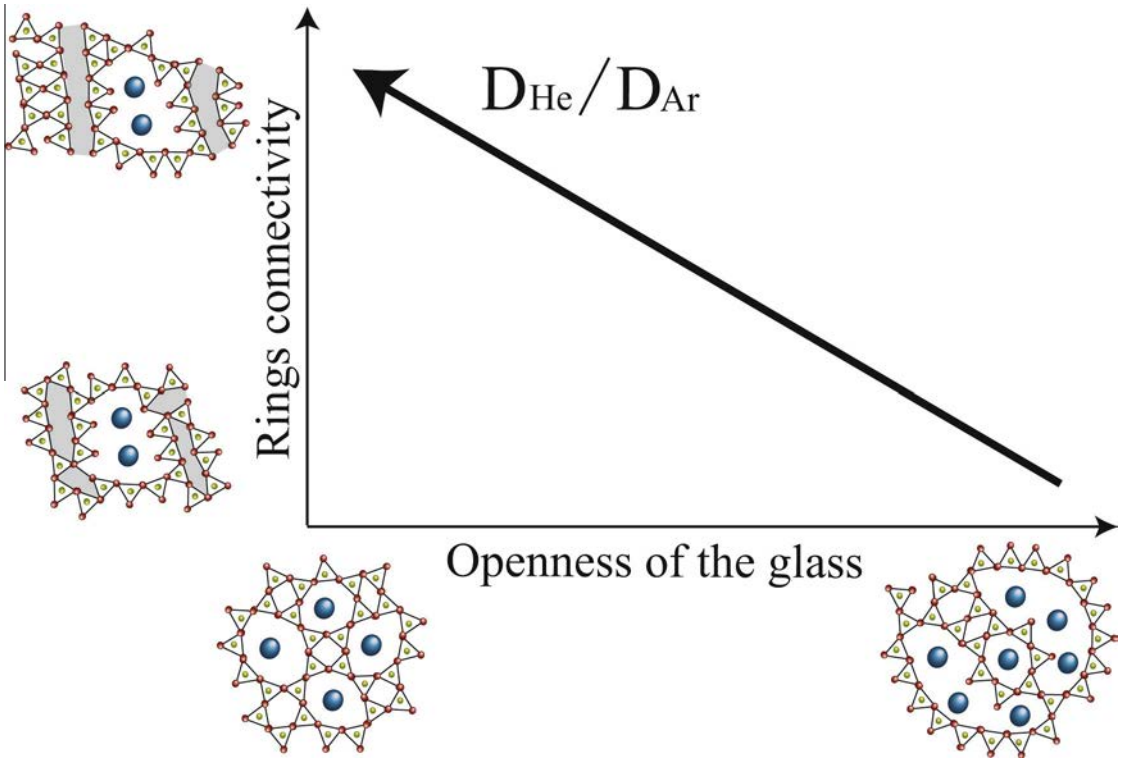


Fig. 10. Schematic evolution of relative He and Ar diffusion as a function of the connectedness of ring structures (y-axis) and the openness of the silicate network (x-axis). Symbols are as follows: large blue circles are the alkali or alkaline earth atoms, medium sized, red circles are the oxygens (bridging or non-bridging), and small yellow circles are the network formers cation. When the concentration and connectedness of rings are high, diffusion of He is enabled through the channels created by the rings whereas the large Ar atoms are unable to exploit these channels, resulting in high D_{He}/D_{Ar}. Open glass structures do not discriminate between He and Ar atoms, therefore the D_{He}/D_{Ar} reduces.

be more readily influenced by the extent of Si–O bond rupturing close to the T_g.

He diffusion in the G2 silica-rich glass and the G1 silica-poor glass, and generally in different silica content glasses, follows this pattern (Fig. 9a) and presumably the more rapid He diffusion in G2 glass reflects the additional connectivity of the glass structure.

It seems likely that the microchannels that are available for He diffusion are too small to allow passage to the larger Ar atoms. As a result, Ar diffusion is instead governed by the entire structure of the glass network (ionic porosity) (Fig. 10). Therefore contrasting behavior is observed for Ar and He diffusion through glass networks where creation/destruction of microchannels is critical to He diffusion whereas the ionic porosity (i.e. the integrated free volume in the glass or melt structure) is the determining factor for Ar diffusion.

4.4. Diffusive fractionation of Ar isotopes

According to Graham's law, the rate of diffusion of one gas in another or in air is approximately inversely proportional to the square root of its molecular weight. In the case of two isotopes A and B of a noble gas, the law can be written:

$$\frac{D_A}{D_B} = \left(\frac{M_B}{M_A}\right)^{\beta} \quad (8)$$

where D_A, D_B and M_A, M_B are the diffusion coefficients and the masses of isotopes A and B, respectively, and $\beta = 0.5$ for gases. It is generally assumed that diffusion of different isotopes of a single noble gas through solids (glasses, crystals) follows a similar law (Craig and Lupton, 1976; Kaneoka, 1980; Burnard and Harrison, 2005; Yamamoto et al., 2009; Pinti et al., 1999; Ruzié and Moreira, 2010). The fundamental assumption behind Graham's law is that the diffusing species (^{36}Ar and ^{40}Ar in our case) share the same kinetic energy:

$$1/2M_A V_A^2 = 1/2M_B V_B^2 \quad (9)$$

While this is true (and has frequently been experimentally demonstrated to be the case) for diffusion in the gas phase, in the case of crystals and glasses interaction of the gases with the crystalline or glass framework invalidates this assumption: there are no ^{36}Ar – ^{40}Ar collisions which redistribute kinetic energy.

According to Graham's law, ^{36}Ar should diffuse 5% faster than ^{40}Ar if β is set to 0.5 in Eq. (8): $D^{40}Ar/D^{36}Ar = (36/40)^{1/2} = 0.95$ (Fig. 5). Our data for glass G1 at high temperatures ($T > 1040$ K) suggest that ^{36}Ar diffuses only 2–3% faster than ^{40}Ar (Fig. 5), implying that β is less

than 0.5: $\beta \sim 0.23$. The average value of our $D^{40}Ar/D^{36}Ar$ data for $T > 1040$ K is, however, equal to 0.98 ± 0.14 ($2-\sigma$), so it is equal within error to 0.95.

The low temperature Ar diffusion data ($1003 \leqslant T < 1040$ K) suggest that isotopic fractionation of Ar isotopes may be temperature dependent, with fractionation increasing significantly at low temperatures (Fig. 5): $D^{40}Ar/D^{36}Ar$ rapidly decreased with decreasing temperature, from near unity at $T > 1040$ K to 0.76 close to T_g ($T = 1003$ K). We note that there is significant uncertainty associated with Ar diffusivity measurements at low temperatures as they correspond to relatively low fractions of gas released ($F < 6\%$). In the Arrhenius diagram (Fig. 4), the low-T Ar data for glass G1 define a linear trend that is much steeper than the high temperature linear trend. At present, we don't know if this steeper slope is due to structural changes close to the glass transition or if it is an experimental artifact. Because of this uncertainty and because we did not replicate the experiment, the strong kinetic fractionation of Ar isotopes close to the glass transition temperature is a preliminary result that must be considered with caution.

Temperature dependent fractionation has already been observed for other elements, for example for Li tracer diffusion in pyroxenes by Richter et al. (2014). Trull and Kurz (1999) observed that ^{3}He and ^{4}He diffusion in basaltic glass is also temperature dependent, with β varying between 1.06 and 1.10 between room temperature and 773 K respectively, well below the predicted value (1.15) given by the inverse square root of mass relation. However, our data shows that the ratio $D^{40}Ar/D^{36}Ar$ decreases with increasing temperature (for temperatures below 1040 K). This contradicts Trull and Kurz (1999) observations for He where the light isotope (^{3}He) diffuses progressively more rapidly relative to the heavy isotope (^{4}He) at higher temperatures. Conversely, Shuster et al. (2004) reported no significant difference between the diffusion of ^{3}He and ^{4}He in Durango apatite between 400 and 600 K. These conflicting observations may be related to different diffusion mechanisms resulting from different temperature domains and different materials (glass vs. crystal) as already suggested by Shuster et al. (2004). Nevertheless, all these observations strongly suggest that it is inappropriate to apply Graham's law to noble gas diffusion in solid materials.

4.5. Geological applications

These experiments considerably impact our understanding of how the noble gases diffuse through solids, particularly through silicate glasses. While these observations have implications for several aspects of noble gas geochemistry (thermochronology, fractionation during magmatic degassing), we focus here on post-eruptive diffusion of noble gases into and out of volcanic glasses and on early partial melting of clinopyroxene crystals.

4.5.1. Pumices

Kaneoka (1980), Pinti et al. (1999) and Ruzié and Moreira (2010) demonstrated that atmosphere-derived noble gases are trapped in bubbles in pumices, recording both isotopic and abundance fractionations resulting from a diffusive process. Two different models were proposed to account for this fractionation: Pinti and coworkers (1999) proposed that atmospheric noble gases diffuse through a glass shell (i.e. post eruption) while Ruzié and Moreira (2010) claimed that Ar diffusion through the glass shell would be too slow, concluding that the fractionation process must have occurred in the magmatic liquid, prior to the eruption. In both studies, the authors used relative noble gas diffusivities estimated using Graham's law to constrain their models due to the lack of experimental diffusion data.

Although our synthetic compositions do not match those of pumices, we can nevertheless better constrain the process of post-eruptive diffusion of noble gases by applying our experimental data. Ruzié and Moreira (2010) demonstrated that diffusion at low (ambient) temperatures were too slow to permit heavy (Ne and Ar) noble gases to significantly diffuse through 10 μm glass walls during the few years elapsed since the eruption that produced the pumice. They did not consider, however, the case of diffusion occurring during pumice cooling. The diffusion coefficients of Ne and Ar at 1100 K are equal to $D(Ne) = 5.1 \times 10^{-10}$ cm^2 s^{-1} and $D(Ar) = 6.2 \times 10^{-11}$ cm^2 s^{-1}. With these coefficients, the durations required for Ne and Ar to diffuse through 10 μm glass walls fall to ~30 min and ~4 h, respectively. If we consider now a glass shell thickness of 1 μm (the lower limit in pumices (Whitman and Sparks, 1986)), the atmospheric noble gas diffusion would be extremely rapid and take only ~20 s for Ne and ~2 min for Ar at 1100 K, which are reasonable time scales for a sustained temperature of 1100 K.

It is important to bear in mind that the noble gas diffusion coefficients above correspond to glass G1, which is depleted in SiO_2 compared to pumice composition. The SiO_2 content tends generally to increase the diffusivity (Shelby, 1974a; Shelby and Eagan, 1976; Jambon and Shelby, 1980; Carroll, 1991; Roselieb et al., 1992), and so the time scales required for atmospheric contamination may even be lower than the above estimates.

4.5.2. Applications to Ar diffusion in minerals

Non-Arrhenian diffusion of Ar has been observed in crystals at temperatures approaching (but nevertheless well below) their melting point. This was well illustrated recently by Cassata et al. (2011) who observed a several orders of magnitude increase in Ar diffusivities in clinopyroxene (CPX) at ~1500 K relative to well defined Arrhenius behavior at lower temperatures. They called this effect "argon bursting", and attributed it to early partial melting of the crystalline network along structural defects. Early partial melting of CPX has been reported by Doukhan et al. (1993) and Richet et al. (1994) (despite the different conclusions of these papers) among others. We propose that early partial melting results in modifications of the crystal network that are somehow similar to that observed in glasses as the T_g is approached and that lead to the Ar bursting observed by Cassata et al. (2011). If this is the case, Ar bursting could be modeled using the modified VTF equation (Eq. (6)). As shown in Fig. 11, it is possible to fit reasonably well the jump in Ar diffusivity using Eq. (6)

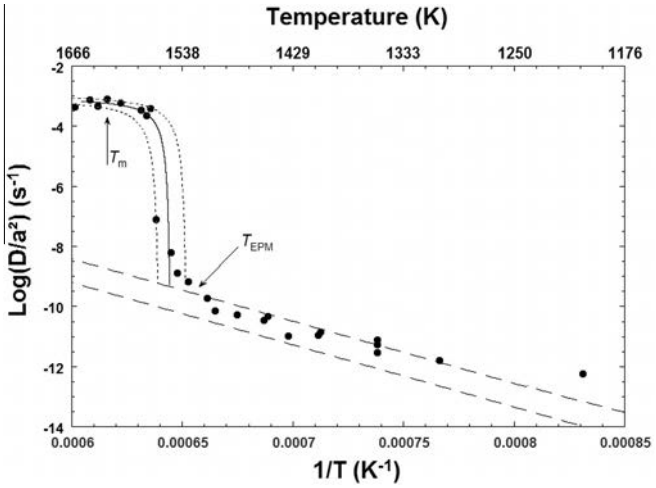


Fig. 11. Diffusion of Ar through clinopyroxene CPX-13 (step, heating data from Cassata et al. (2011)) shows a distinct departure from an Arrhenius relation at ~1530 K. This is attributed to early partial melting (EPM) as the CPX melting point (T_M) is approached. It is possible to model this departure from Arrhenian behavior as a modified VTF relationship, suggesting that the increased Ar release could be due to a relaxation of the crystal lattice at temperatures below the mineral melting temperature. The two dotted lines are the uncertainties in the VTF fit due to the resolution of the experimental data. The two dashed lines are the Arrhenius relations given by Cassata et al. (2011) for $T < T_{EPM}$.

with $A_1/a^2 = 9.6 \times 10^{-4}$ s^{-1}, $B_1 = 0.31$ kJ mol^{-1}, $C = 4.2 \times 10^{-5}$ kJ mol^{-1} and $T_2 = 1550$ K. In other words, the CPX crystal lattice starts to exhibit slight structural rearrangements at temperatures below the liquidus, which are correlated to small structural free volume modifications. Moreover, Ubbelohde (1978) proposed that the "pre-melting" precursor could be due to increasing ion mobility within the mineral lattice, consistent with the network relaxation concept.

5. SUMMARY

Step heating of noble gas doped silicate glasses over the temperature interval 423–1198 K displays complex noble gas (He, Ne and Ar) diffusion behavior. At low temperatures, the diffusivities conform to traditional Arrhenius behavior with well-defined activation energies (E_a) and pre-exponential factors (D_0/a^2). The activation energy increases with mass (from He to Ne; Ar diffusion was not measured at low temperatures) for Arrhenian regimes. At higher temperatures, however, the He and Ne diffusion becomes clearly non-Arrhenian. A modified VTF law is proposed where a second pseudo-activation energy is added to the exponential term in order to account for this non-linearity in a diagram of Log(D/a^2) vs $1/T$: the modified VTF law reproduces well the observations.

There are three different diffusion regimes which are interpreted as follows:

1. Low temperature regime. Temperatures are sufficiently low that the glass network is immobile and traditional temperature activated (Arrhenian) diffusion occurs.
2. Mid-temperature regime. As the glass transition (T_g) is approached, the glass network is no longer rigid, allowing modification of the free volume distribution within the glass. Thus noble gas diffusion depends not only on activation of the noble gas atoms but also on the relaxation of the free volume, resulting in a second activation term in the modified VTF relation. O^{2-} diffusivities calculated above T_g are sufficient to modify the distribution of the free volume within the glass over the time scale of the step heating experiments.
3. High Temperature regime. At temperatures above T_g, the silicate network softens and melts. Only ^{20}Ne and ^{4}He clearly show non-Arrhenian behavior in the high temperature region ($T > T_g$) of the step heating profile.

These new diffusion results are used to estimate the time scales required to develop fractionated atmospheric noble gas signatures in pumices and to discuss the effect of early partial melting of clinopyroxene crystals on Ar diffusion. We show that the modified VTF law can also be used to describe Ar diffusion in clinopyroxene at high temperatures, suggesting that slight modifications to the crystal lattice have similar effects on Ar diffusivity as the modifications of the silicate glass network close to the glass transition.

ACKNOWLEDGEMENTS

Charles Le Losq is warmly thanked for discussion and comments on the manuscript. We would like to thank Marissa Tremblay and an anonymous reviewer for their constructive comments, and David Shuster and Marc Norman for editing our manuscript. This work benefited from a financial support from the Agence Nationale de la Recherche [DEGAZMAG project, contract no. ANR 2011 Blanc SIMI 5-6 003] and a Région Lorraine stipend for JVRA.

REFERENCES

Behrens H. (1992) Na and Ca tracer diffusion in plagioclase glasses and supercooled melts. *Chem. Geol.* **96**, 267–275.

Behrens H. (2010) Noble gas diffusion in silicate glasses and melts. *Rev. Mineral. Geochem.* **72**, 227–267.

Boettcher S. L., Guo Q. and Montana A. (1989) A simple device for loading gases in high-pressure experiments. *Am. Mineral.* **74**, 1383–1384.

Burnard P. and Harrison D. (2005) Argon isotope constraints on modification of oxygen isotopes in Iceland Basalts by surficial processes. *Chem. Geol.* **216**, 143–156.

Braedt M. and Frischat G. H. (1988) Sodium self diffusion in glasses and melt of system Na_2O–Rb_2O–SiO_2. *Phys. Chem. Glasses* **29**, 214–218.

Brebec G., Seguin R., Sella C., Bevenot J. and Martin J. C. (1980) Diffusion du silicium dans la silice amorphe. *Acta Metall.* **28**, 327–333.

Caillot E., Duclot M. J., Souquet J. L. and Levy M. (1994) A unified model for ionic transport in alkali disilicates below and above the glass transition. *Phys. Chem. Glasses* **35**, 22–27.

Carroll M. R. (1991) Diffusion of Ar in rhyolite, orthoclase and albite composition glass. *Earth Planet. Sci. Lett.* **103**, 156–168.

Carslaw H. S. and Jaeger J. C. (1959) *Conduction of heat in solids*, second ed. Clarendon Press, Oxford, p. 505.

Cassata W. S., Renne P. R. and Shuster D. L. (2011) Argon diffusion in pyroxene: implication for thermochronometry and mantle degassing. *Earth Planet. Sci. Lett.* **304**, 407–416.

Chakraborty S. (1995). Diffusion in silicate melts. In *Reviews in Mineralogy*, (ed. J. F., Stebbins, P. F., McMillan, D. B., Dingwell), Mineralogical society of America, Washington D.C., 32, pp. 411–503.

Cheradame H. (1982). "IUPAC Macromolecules", (eds. H. Benoit and P. Rempp), Pergamon Press, Oxford and New York, p 251.

Cohen M. H. and Grest G. S. (1979) Liquid–glass transition, a free–volume approach. *Phys. Rev. B* **20**, 1077.

Craig H. and Lupton J. E. (1976) Primordial neon, helium, and hydrogen in oceanic basalts. *Earth Planet. Sci. Lett.* **31**, 369–385.

Crank J. (1975) *The Mathematics of Diffusion*, second ed. Clarendon Press, Oxford, p. 413.

De Berg K. C. and Lauder I. (1980) Oxygen tracer diffusion in a potassium silicate glass above the transformation temperature. *Phys. Chem. Glasses* **21**, 106–109.

Doolittle A. K. (1951) Studies in Newtonian Flow. II. The dependence of the viscosity of liquids on free-space. *J. Appl. Phys.* **22**, 1471–1475.

Doremus R. H. (1975) *Glass science*. John Wiley and Son, N.Y., p. 349.

Doukhan N., Doukhan J. C., Ingrin J., Jaoul O. and Raterron P. (1993) Early partial melting in pyroxenes. *Am. Mineral.* **78**, 1246–1256.

Dunn T. (1982) Oxygen diffusion in three silicate melts along the join diopside–anorthite. *Geochim. Cosmochim. Acta* **46**, 2293–2299.

Farley K. A., Reiners P. X. and Nenow V. (1999) An apparatus for high–precision Helium diffusion measurements from minerals. *Anal. Chem.* **71**, 2059–2061.

Fechtig H. and Kalbitzer S. (1966). The Diffusion of Argon in Potassium-Bearing Solids, in Potassium Argon Dating. Berlin–Heidelberg: Springer-Verlag, p. 68–107.

Frischat G. H., Poggemann J. F. and Heide G. (2004) Nanostructure and atomic structure of glass seen by atomic force microscopy. *J. Non-Cryst. Solids* **345**, 197–202.

Fulcher G. S. (1925) Analysis of recent data of the viscosity of glasses. *J. Am. Ceram. Soc.* **8**, 339–355.

Geyer U., Johnson W. L., Schneider S., Qiu Y., Tombrello T. A. and Macht M. P. (1996) Small atom diffusion and breakdown of the Stokes-Einstein relation in the supercooled liquid state of the Zr46. 7Ti8. 3Cu7. 5Ni10Be27. 5 alloy. *Appl. Phys. Lett.* **69**, 2492–2494.

Greaves G. N. (1985) Exafs and the structure of glass. *J. Non-Cryst. Solids* **71**, 203–217.

Greaves G. N. (1989) EXAFS, glass structure and diffusion. *Philoso. Mag. Part B* **60**, 793–800.

Greaves G. N., Fontaine A., Lagarde P., Raoux D. and Gurman S. J. (1981) Local structure of silicate glasses. *Nature* **293**, 611–616.

Greaves G. N. and Ngaï K. L. (1995) Reconciling ionic transport with atomic structure in oxide glasses. *Phys. Rev. B.* **52**, 6358.

Iacono M. G., Paonita A., Rizzo A., Scaillet B. and Gaillard F. (2010) Noble gas solubilities in silicate melts: new experimental results and a comprehensive model of the effects of liquid composition, temperature and pressure. *Chem. Geol.* **279**, 145–157.

Jambon A. and Shelby J. S. (1980) Helium diffusion and solubility in obsidians and basaltic glass in the range 200–300 ° C. *Earth Planet. Sci. Lett.* **51**, 206–214.

Kaneoka I. (1980) Rare gas isotopes and mass fractionation: an indicator of gas transport into or from a magma. *Earth Planet. Sci. Lett.* **48**, 284–292.

Kargl F. and Meyer A. (2008) Na–relaxation and intermediate range structure in sodium–potassium silicate melts. *Chem. Geol.* **256**, 278–285.

Koros P. J. and King T. B. (1962) The self–diffusion of oxygen in a lime–silica–alumina slag. *Trans. Metal. Soc. AIME* **224**, 299–306.

Kress V. C. and Carmichael I. S. E. (1991) The compressibility of silicate liquids containing Fe_2O_3 and the effect of composition temperature, oxygen fugacity and pressure on their redox states. *Contrib Mineral. Petrol.* **108**, 82–92.

Kurz M. D. and Jenkins W. J. (1981) The distribution of helium in oceanic basalt glasses. *Earth Planet. Sci. Lett.* **53**, 41–54.

Laporte D., Toplis M. J., Seyler M. and Devidal J. L. (2004) A new experimental technique for extracting liquids from peridotite at very low degrees of melting: application to partial melting of depleted peridotite. *Contrib. Mineral. Petrol.* **146**, 463–484.

Le Losq C. and Neuville D. R. (2013) Effect of the Na/K mixing on the structure and the rheology of tectosilicate silica–rich melts. *Chem. Geol.* **346**, 57–71.

Le Losq C., Neuville D. R., Florian P., Henderson G. S. and Massiot D. (2014) The role of Al^{3+} on rheology and structural changes of sodium silicate and aluminosilicate glasses and melts. *Geochim. Cosmochim. Acta* **126**, 495–517.

Macedo P. B. and Litovitz T. A. (1965) On the relative roles of free volume and activation energy in the viscosity of liquids. *J. Chem. Phys.* **42**, 245.

Machin J. S., Yee T. B. and Hanna D. L. (1952) Viscosity Studies of System CaO–MgO–Al_2O_3–SiO_2: III, 35, 45, and 50% SiO_2. *J. Am. Ceram. Soc.* **35**, 322–325.

Magnien V., Neuville D. R., Cormier L., Roux J., Hazemann J. L., Pinet O. and Richet P. (2006) Kinetics or iron redox reactions insilicate liquids: a high–temperature X–ray absorption and Raman spectroscopy study. *J. Nucl. Mater.* **253**, 190–195.

Magnien V., Neuville D. R., Cormier L., Roux J., Hazemann J. L., De Ligny D., Pascarelli D., Pinet O. and Richet P. (2008) Kinetics of iron redox reactions in silicate melts: the effect of temperature and alkali cation. *Geochim. Cosmochim. Acta* **72**, 2157–2168.

May H. B., Lauder I. and Wollast R. (1974) Oxygen diffusion coefficient in alkali silicates. *J. Am. Ceram. Soc.* **47**, 197–200.

McDougall, I. and Harrison, T. M., (1999). Geochronology and Thermochronology by the $^{40}Ar/^{39}Ar$. Method Oxford University Press, p.269.

Meesters A. G. C. A. and Dunai T. J. (2002) Solving the production–diffusion equation for finite diffusion domains of

various shapes: Part I. Implications for low–temperature (U–Th)/He thermochronology. *Chem. Geol.* **186**, 333–344.
Meyer J. C., Paillet M., Michel T., Moréac A., Neumann A., Duesberg G. S. and Sauvajol J. L. (2005) Raman modes of index–identified freestanding single–walled carbon nanotubes. *Phys. Rev. Lett.* **95**, 217401.
Miyamoto T. and Shibata K. (1973) Free-volume model for ionic conductivity in polymers. *J. Appl. Phys.* **42**, 5372.
Moreira M. (2013) Noble gas constraints on the origin and evolution of Earth's volatiles. *Geochem. Perspect.* **2**, 229–230.
Muehlenbachs K. and Kurisho I. (1974). Oxygen isotope exchange and equilibration of silicates with CO_2 and O_2. Carnegie Institution of Washington Yearbook, **73**, 232–236.
Mysen B. O., Virgo D. and Seifert F. A. (1984) Redox equilibria of iron in alkaline earth silicate melts: relationships between melt structure, oxygen fugacity, temperature and properties of iron–bearing silicate liquids. *Am. Mineral.* **69**, 834–848.
Nakayama G. S. and Shackelford J. F. (1990) Solubility and diffusivity of Argon in vitreous silica. *J. Non-Cryst. Solids* **126**, 249–254.
Neuville D. R., (1992). Etude des propriétés thermodynamiques et rhéologiques des silicates fondus. Thèse de Doctorat. Université Paris 7, p241.
Neuville D. R. (2006) Viscosity, structure and mixing in (Ca, Na) silicate melts. *Chem. Geol.* **229**, 28–41.
Neuville D. R. and Richet P. (1991) Viscosity and mixing in molten (Ca, Mg) pyroxenes and garnets. *Geochim. Cosmochim. Acta* **55**, 1011–1021.
Oishi Y., Terai R. and Ueda U. (1975) Oxygen diffusion in liquid silicates and relation to their viscosity. In *Mass Transport Phenomena in Ceramics* (eds. A. Cooper and A. Heuer). Plenum Press, New York, pp. 297–310.
Parks G. S. and Huffman H. M. (1928) Studies on glass. I. The transition between the glassy and liquid states in the case of some simple organic compound. *J. Phys. Chem.* **31**, 1842–1855.
Perkins W. G. and Begeal D. R. (1971) Diffusion and permeation of He, Ne, Ar, Kr and D_2 through silicon oxide thin films. *J. Chem. Phys.* **54**, 1683–1694.
Pinti D., Wada N. and Matsuda J. (1999) Neon excess in pumice: volcanological implications. *J. Vol. Geotherm. Res.* **88**, 279–289.
Reichenberg D. (1953) Properties of ion–exchange resins in relation to their structure. III. Kinetics of exchange. *Am. Chem. Soc.* **75**, 589–897.
Reynolds M. B. (1957) Diffusion of Argon in potassium–lime–silica glass. *J. Am. Ceram. Soc.* **40**, 395–398.
Richet P., Ingrin J., Mysen B. O., Courtial P. and Guillet P. (1994) Premelting effects in minerals: an experimental study. *Earth Planet. Sci. Lett.* **121**, 589–600.
Richter F., Watson B., Chaussidon M., Mendybaev R. and Ruscitto D. (2014) Lithium isotope fractionation by diffusion in minerals. Part 1: Pyroxenes. *Geochim. Cosmochim. Acta* **126**, 352–370.
Roger W. A., Buritz R. S. and Alpert D. (1954) Diffusion coefficient, solubility, and permeability for helium in glass. *J. Appl. Phys.* **25**, 868–875.
Roselieb K., Rammensee W., Büttner H. and Rosenhauer M. (1992) Solubility and diffusion of noble gases in vitreous albite. *Chem. Geol.* **96**, 241–266.
Russell J. K., Giordano D. and Dingwell D. B. (2003) High–temperature limits on viscosity of non–Arrhenian silicate melts. *Am. Mineral.* **88**, 1390–1394.
Ruzié L. and Moreira M. (2010) Magma degassing process during Plinian eruptions. *J. Volcanol. Geotherm. Res.* **192**, 142–150.
Sasabe M. and Goto K. S. (1974) Permeability, diffusivity and solubility of the oxygen in liquid slag. *Metal. Trans.* **5**, 2225–2233.
Shelby J. E. (1974) Helium diffusion and solubility in K_2O–SiO_2 glasses. *J. Am. Ceram. Soc.* **54**, 236–263.
Shelby J. E. and Eagan R. J. (1976) Helium migration in sodium aluminosilicate glasses. *J. Am. Ceram. Soc.* **59**, 420–425.
Shuster D. L., Farley K. A., Sisterson J. M. and Burnett D. S. (2004) Quantifying the diffusion kinetics and spatial distribution of radiogenic ^{4}He in mineral containing proton–induced ^{3}He. *Earth Planet. Sci. Lett.* **217**, 19–32.
Sparks R. S. J. (1978) The dynamics of bubble formation and growth in magmas: a review and analysis. *J. Volcanol. Geotherm. Res.* **3**, 1–37.
Strausser C. A., Thomsen M. W., Yoder C. H. and Schaeffer C. D. (2007). Data Tables for General, Organic and Physical Chemistry. second ed. (a sixty–page pamphlet of data tables for use in chemistry courses).
Sweets D. E., Lee R. W. and Frank R. C. (1961) Diffusion coefficient for helium in fused quartz. *J. Chem. Phys.* **34**, 17–22.
Tarjus G. and Kivelson D. (1995) Breakdown of the Stokes-Einstein relation in supercooled liquids. *J. Chem. Phys.* **103**, 3071.
Tammann G. and Hesse W. (1926) Die abhângigkeit der viskositât von der temperature bei unterkuhlten flussigkeiten. *Zeitzchriift fur anorganische allgemeine chemie* **156**, 245–257.
Terrai R. and Oishi Y. (1977) Self-diffusion of oxygen in soda–lime–silicate glass. *Glastech. Ber.* **50**, 68–73.
Trull T. W. and Kurz M. D. (1999) Isotopic fractionation accompanying helium diffusion in basaltic glass. *J. Mol. Struct.* **485**, 555–567.
Turnbull D. and Cohen M. H. (1961) Free-volume model of the amorphous phase: glass transition. *J. Chem. Phys.* **34**, 120–125.
Turnbull D. and Cohen M. H. (1970) On the free-volume model of the liquid–glass transition. *J. Chem. Phys.* **52**, 3038–3041.
Ubbelohde A. R. (1978) *The Molten State of the Matter*. John Wiley and Son, New York.
Vogel H. (1921) Das temperature–abhângigketsgesetz der viskoditât von flüssigkeiten. *Physikalische zeitschrift* **22**, 645–646.
Wendlandt R. F. (1980) Oxygen diffusion in basalt and andesite melts. *EOS* **61**, 1142.
Whitman A. G. and Sparks R. S. J. (1986) Pumice. *Bull. Volcanol.* **48**, 209–233.
Williams M. L., Landel R. F. and Ferry J. D. (1955) The temperature dependence of relaxation mechanisms in amorphous polymers and other glass-forming liquids. *J. Am. Chem. Soc.* **77**, 3701–3707.
Yamamoto J., Nishimura K., Sugimoto T., Takemura K., Takahata N. and Sano Y. (2009) Diffusive fractionation of noble gases in mantle with magma channels: origin of low He/Ar in mantle–derived rocks. *Earth Planet. Sci. Lett.* **280**, 167–174.
Yinnon H. and Cooper A. R. (1980) Oxygen diffusion in multicomponent glass forming silicates. *Phys. Chem. Glasses* **21**, 204–211.